25. Murakami T, Nakashima K, Yarimitsu S, et al. Effectiveness of adsorbed film and gel layer in hydration lubrication as adaptive multimode lubrication mechanism for articular cartilage. *Proc IMechE Part J: J Engineering Tribology* 2011; 225: 1174–1185.
26. Williams PA, Yamamoto K, Masaoka T, et al. Highly crosslinked polyethylenes in hip replacements: improved wear performance or paradox? *Tribol Trans* 2007; 50: 277–290.
27. Tomita N, Kitakura T, Onmori N, et al. Prevention of fatigue cracks in ultrahigh molecular weight polyethylene joint components by the addition of vitamin E. *J Biomed Mater Res Part B* 1999; 48: 474–478.
28. Moro T, Takatori Y, Ishihara K, et al. Surface grafting of artificial joints with a biocompatible polymer for preventing periprosthetic osteolysis. *Nat Mater* 2004; 3: 829–836.
29. Issac GH, Thompson J, Williams S, et al. Metal-on-metal bearings surfaces: materials, manufacture, design, optimization, and alternatives. *Proc IMechE Part H: J Engineering in Medicine* 2006; 220: 119–133.
30. Früh HJ, Willmann G and Pfaff HG. Wear characteristics of ceramic-on-ceramic for hip endoprostheses. *Biomaterials* 1997; 18: 873–876.
31. Unsworth A, Pearcy MJ, White EFT, et al. Soft layer lubrication of artificial hip joints. *Proc IMechE Part C: J Mechanical Engineering Science* 1987; 219(87): 715–724.
32. Murakami T, Sawae Y, Higaki H, et al. Adaptive multimode lubrication in knee prostheses with artificial cartilage during walking. In: Dowson D, Taylor CM, Childs THC, Dalmaz G, Berthier Y, Flamand L, Georges J-M and Lubrecht AA (eds) *Elastohydrodynamics '96: Fundamentals and applications in lubrication and traction*. Amsterdam: Elsevier Science, 1997, pp.371–382.
33. Sasada T. Biomechanics and biomaterials–friction behaviour of an artificial articular cartilage. In: *Transactions of the 3rd world biomaterials congress*, Kyoto, Japan, 21–25 April 1988, vol. 11, p.6.
34. Oka M, Ushio K, Kumar P, et al. Development of artificial cartilage. *Proc IMechE Part H: J Engineering in Medicine* 2000; 214: 59–68.
35. Nakashima K, Sawae Y and Murakami T. Study of wear reduction mechanisms of artificial cartilage by synergistic protein boundary film formation. *JSME Int J* 2005; 48(4): 555–561.
36. Yarimitsu S, Nakashima K, Sawae Y, et al. Study on mechanisms of wear reduction of artificial cartilage through in situ observation on forming protein boundary film. *Tribol Online* 2007; 2(4): 114–119.
37. Yarimitsu S, Nakashima K, Sawae Y, et al. Effect of lubricant composition on adsorption behavior of proteins on rubbing surface and stability of protein boundary film. *Tribol Online* 2008; 3(4): 238–242.
38. Yarimitsu S, Nakashima K, Sawae Y, et al. Influence of lubricant composition on forming boundary film composed of synovia constituents. *Tribol Int* 2009; 42: 1615–1623.
39. Kobayashi M, Chang YS and Oka M. A two year in vivo study of polyvinyl alcohol-hydrogel (PVA-H) artificial meniscus. *Biomaterials* 2005; 26: 3243–3248.
40. Nakashima K, Sawae Y, Tsukamoto N, et al. Wear behavior of an artificial cartilage material for hemiarthroplasty. In: *Proceedings of the 6th world congress of biomechanics, WCB 2010*, Singapore, 1–6 August. *IFMBE Proc* 2010; 31: 1169–1172.
41. Murakami T, Sakai N, Sawae Y, et al. Influence of proteoglycan on time-dependent mechanical behaviors of articular cartilage under constant total compressive deformation. *JSME Int J Ser C* 2004; 47: 1049–1055.
42. Hosoda N, Sakai N, Sawae Y, et al. Depth-dependence and time-dependence in mechanical behaviors of articular cartilage unconfined compression test under constant total deformation. *J Biomech Sci Eng* 2008; 3(2): 209–220.
43. Jurvelin JS, Bushmann MD and Hunziker EB. Mechanical anisotropy of the human knee articular cartilage in compression. *Proc IMechE Part H: J Engineering in Medicine* 2003; 217: 215–219.
44. Li LP, Soulhat J, Buschmann MD, et al. Nonlinear analysis of cartilage in unconfined ramp compression using a fibril reinforced poroelastic model. *Clin Biomech* 1999; 14: 673–682.
45. Wu JZ, Herzog W and Epstein M. Evaluation of the finite element software ABAQUS for biomechanical modelling of biphasic tissues, technical note. *J Biomechanics* 1998; 31: 165–169.
46. Sakai N, Hosoda N, Hagiwara Y, et al. Analyses of functional mechanism of articular cartilage (in Japanese). *Biomechanisms* 2012; 21: 251–263.
47. Murakami T, Sawae Y, Nakashima K, et al. Micro- and nanoscopic biotribological behaviours in natural synovial joints and artificial joints. *Proc IMechE Part J: J Engineering Tribology* 2007; 221: 237–245.
48. Pawaskar SS, Jin ZM and Fisher J. Modelling of fluid support inside articular cartilage during sliding. *Proc IMechE Part J: J Engineering Tribology* 2007; 221: 165–174.
49. Murakami T, Yarimitsu S, Nakashima K, et al. Time-dependent frictional behaviours in hydorogel artificial cartilage materials. In: *Proceedings of the 6th international biotribology forum (Biotribology Fukuoka 2011)*, Fukuoka, Japan, 5 November 2011, pp.65–68.
50. Nakashima K, Sawae Y and Murakami T. Influence of protein conformation on frictional properties of poly (vinyl alcohol) hydrogel for artificial cartilage. *Tribol Lett* 2007; 26: 145–151.

Biochemical and Biophysical Research Communications 424 (2012) 724–729

Contents lists available at SciVerse ScienceDirect

Biochemical and Biophysical Research Communications

journal homepage: www.elsevier.com/locate/ybbrc

Effects of both vitamin C and mechanical stimulation on improving the mechanical characteristics of regenerated cartilage

Seiji Omata [a,*], Shogo Sonokawa [b], Yoshinori Sawae [c], Teruo Murakami [d]

[a] Department of Biomedical Engineering, Graduate School of Biomedical Engineering, Tohoku University, Sendai, Miyagi, Japan
[b] Department of Mechanical Engineering, Graduate School of Engineering, Kyushu University, Fukuoka, Japan
[c] Department of Mechanical Engineering, Faculty of Engineering, Kyushu University, Fukuoka, Japan
[d] Advanced Biomaterials Division, Research Center for Advanced Biomechanics, Kyushu University, Fukuoka, Japan

ARTICLE INFO

Article history:
Received 22 June 2012
Available online 16 July 2012

Keywords:
Regenerated-cartilage tissue
Interconnection
Extracellular matrix network
Mechanical property
Mechanical stimulation

ABSTRACT

The present work describes the influence of both vitamin C (VC) and mechanical stimulation on development of the extracellular matrix (ECM) and improvement in mechanical properties of a chondrocyte–agarose construct in a regenerating tissue disease model of hyaline cartilage. We used primary bovine chondrocytes and two types of VC, ascorbic acid (AsA) as an acidic form and ascorbic acid 2-phosphate (A2P) as a non-acidic form, and applied uniaxial compressive strain to the tissue model using a purpose-built bioreactor. When added to the medium in free-swelling culture conditions, A2P downregulated development of ECM and suppressed improvement of the tangent modulus more than AsA. By contrast, application of mechanical stimulation to the construct both increased the tangent modulus more than the free-swelling group containing A2P and enhanced the ECM network of inner tissue to levels nearly as high as the free-swelling group containing AsA. Thus, mechanical stimulation and strain appears to enhance the supply of nutrients and improve the synthesis of ECM via mechanotransduction pathways of chondrocytes. Therefore, we suggest that mechanical stimulation is necessary for homogenous development of ECM in a cell-associated construct with a view to implantation of a large-sized articular cartilage defect.

1. Introduction

Articular cartilage covers the surface of the ends of bones in synovial capsules and performs the important function of high performance weight-bearing at very low friction and wear in daily activities during a healthy life. The behavior of articular cartilage tissue as a mechanical system is dependent chiefly on an extracellular matrix (ECM), which consists primarily of a protein, called type II collagen (10–20% of the wet weight), and proteoglycans (about 10% of the wet weight) [1]. Steric and electrostatic interactions of ECM molecules in the cartilage tissue occur between the cationic collagen fibers and the anionic proteoglycans to provide a highly charged environment under neutral pH conditions. Although adult articular cartilage is a remarkable load-bearing system, following traumatic injury or under conditions of wear and tear, it lacks the ability of self-repair, which can often lead to osteoarthritis (OA).

Such diseases of hyaline cartilage are a major health problem, especially in industrialized countries with relatively long active life expectancies. At present, no cell-assisted tissue regeneration therapy for the reliable and durable replacement of damaged articular cartilage has been established [2–4]. However, in recent years, tissue engineering has become a promising option for the treatment of OA and has allowed researchers to produce functional replacements for diseased cartilage [5,6]. Developments in therapeutic strategies for damaged cartilage treatment have increasingly focused on the promising technology of cell-assisted repair, which proposes the use of autologous chondrocytes or other cell types to regenerate articular cartilage [4,7].

There is still too little knowledge available to establish a suitable design strategy for reconstructing tissue-engineered cartilage that matches the mechanical properties of natural tissue. In this study, we focused on the relationship between the collagen network and the mechanical properties of a regenerated-cartilage tissue model and showed that the collagen network interconnecting chondrocytes improved the mechanical properties of the tissue to be equivalent to that of scaffold material without chondrocytes if there was no linkage between cells by the ECM network [8]. We used ascorbic acid (AsA), a type of vitamin C (VC), in the culture medium to control collagen synthesis in order to investigate the

* Corresponding author. Address: Sato-Huang/Deguchi Lab. Graduate School of Biomedical Engineering, Tohoku University, 6-6-1, Aoba, Aramaki, Aoba, Sendai, Miyagi 980-8579, Japan.
E-mail address: s_omata@bml.mech.tohoku.ac.jp (S. Omata).

0006-291X/$ - see front matter © 2012 Elsevier Inc. All rights reserved.
http://dx.doi.org/10.1016/j.bbrc.2012.07.019

effect of developing a collagen network on the mechanical properties of the tissue model. However, high concentrations of AsA were found to be toxic to the chondrocytes with no concomitant improvement in mechanical properties.

As for AsA above, we used ascorbic acid 2-phosphate (A2P), a non-acidic form, for suppressing the cytotoxicity and effective development of the mechanical characteristics of the tissue, and demonstrated the relationship between VCs in the culture medium and development of ECM and mechanical properties of the construct. In addition, we thought that applying a compressive deformation to the tissue model would not only improve diffusion of culture medium into the tissue and accelerate the supply of nutrients, but also activate cell-signaling via mechanosensor and mechanotransduction pathways. It is well known that loading mechanical stimuli to regenerated-cartilage tissue and chondrocytes is distinctly important for both enhancing synthesis of ECM and inducing chondrogenesis differentiation of stem cells [9]. Hence, in order to apply a compressive deformation to the tissue model for development of ECM, we made a purpose-built bioreactor capable of applying an uniaxial unconfined compressive strain to individual constructs in an incubator. The purpose of the present study was to investigate the effects of applying both two types of VC and dynamic compression to a regenerated-cartilage tissue model on the mechanical properties and development of the ECM network.

2. Materials and methods

2.1. Sample preparation and tissue culture

Primary bovine chondrocytes were isolated from metacarpophalangeal joints of steers purchased from a butchery using a sequential enzyme digestion method [10]. Full thickness articular cartilage tissue was harvested from the proximal articular surface of the metatarsal bone and finely diced with a scalpel. The finely diced cartilage tissue was enzymatically digested in a 25 unit/mL protease solution (P8811, Sigma, St Louis, MO) for 3 h and subsequently in a 200 unit/mL collagenase solution (C7657, Sigma) for 18 h at 37 °C. Both enzyme solutions were prepared in sterile tissue culture medium consisting of Dulbecco's modified Eagle's medium (DMEM; D5921, Sigma) supplemented with 20 v/v% Fetal Bovine Serum (FBS; 10437–028, Gibco, Carlsbad, CA), 2 mM L-glutamine (G7513, Wako Pure Chemical Industries, Ltd., Osaka, Japan), 100 unit/mL penicillin, 100 μg/mL streptomycin, 0.25 μg/mL amphotericin B (161–23181, Wako), 20 mM Hepes (H0887, Sigma), and 0.85 mM L-ascorbic acid (AsA; A5960, Sigma). The supernatant of the resultant solution was centrifuged to separate chondrocytes at 40 × g for 5 min. The resultant cell pellet was washed twice in fresh culture medium, and then cell number and cell viability were determined using Trypan Blue assay. In this study, Sigma Type VII agarose (A6560, Sigma) was used to prepare a chondrocyte–agarose construct. The agarose powder was dissolved in Earle's Balanced Salts Solution (EBSS; Sigma) at twice the required final concentration (1 w/v%) and mixed with an equal volume of the cell suspension to yield the desired agarose concentration with a final cell density of 1×10^7 cells/mL. The molten cell-agarose solution was poured into an acrylic mold and quenched into gel at 4 °C for 30 min to create cylindrical constructs with a diameter of 4 mm and a height of 2.5 mm. The resultant cell-agarose constructs were placed into a 24-well culture plate and cultured with 1 mL culture medium in an incubator at 37 °C and 5% CO_2. The culture medium was exchanged every 2 days. Several culture media with different VC concentrations, from 2.2 to 32 pmol/10^9 cells, were prepared and used to evaluate the effect of AsA and L-ascorbic acid 2-phosphate magnesium salt (A2P, Wako) concentrations. Culture medium without VC was also used as a control. Each medium is abbreviated as AsA(2.2), A2P(6.4), and A2P(32) hereafter in this paper.

After 1 day of free-swelling culture, the constructs in the experiment group were subjected to uniaxial compression within a purpose-built bioreactor system as shown in Fig. 1. The system permits the application of strain independently in both vertical and horizontal directions to individual constructs using a 24-well plate in a commercially available incubator. The movements were controlled with respective linear variable displacement transducers and linear guide actuators. Strain was applied to the individual constructs through a loading plate, which was attached to the actuator via a jig. Uniaxial cyclic compression up to a maximum amplitude of 15% was applied in a triangular waveform at a frequency of 1 Hz for 6 h and subsequently off-loaded with the plate resting for each construct over the subsequent 18 h. Control constructs were cultured, in contrast, with both upper and lower plates for diffusion through the sides alone.

2.2. Measurement of mechanical property

To examine the influence of VC concentration, cell-agarose constructs were subjected to unconfined compression while immersed in culture medium at room temperature. Individual constructs were tested after culture periods of 22 days. Mechanical tests were

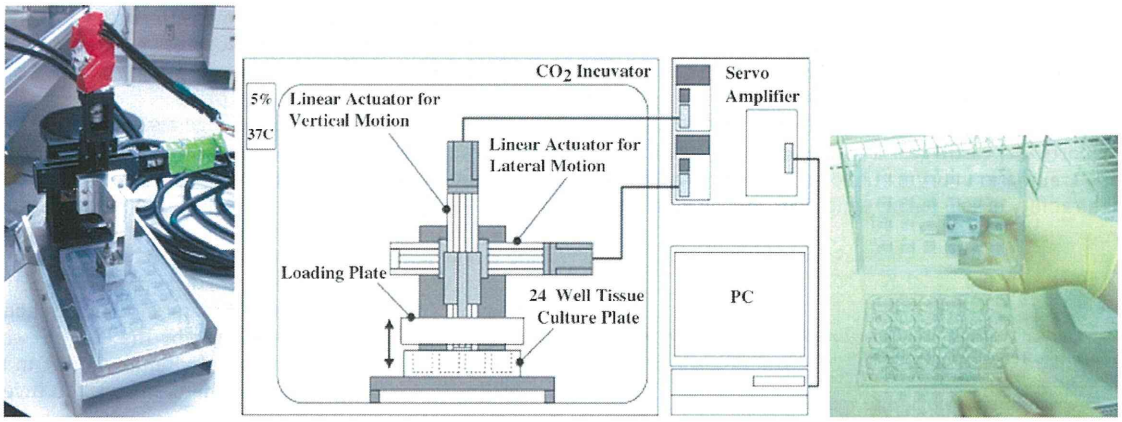

Fig. 1. Photograph (left) and Schematic drawing (center) of mechanical loading system mounted within tissue culture incubator. Loading plate with 22 plungers coupled with a 24-well culture plate (right).

performed with an impermeable stainless steel plunger at a strain rate of 0.5 mm/min up to a strain of 10%, while the load was recorded with a 10 N load sensor. The tangent modulus of the construct was calculated from the slope of a straight-line approximation of the stress–strain curve with a range of 0–15% strain using the least-square method.

2.3. Immunohistology

Separate constructs were used for trichrome immunofluorescence observation to examine the morphological characteristics of the elaborated ECMs, in particular type I collagen, type II collagen and chondroitin sulfate. After the prescribed culture periods, representative constructs were cut into slices with a thickness of approximately 1 mm using a knife. The slices were washed in PBS(−) and subsequently incubated in PBS(−) + 1 w/v% bovine serum albumin (BSA; Wako) for 30 min at 37 °C. These slices were incubated in PBS(−) containing the three monoclonal antibodies (bovine IgG1 isotype anti-type I collagen, Funakoshi, Tokyo, Japan; embryonic chicken IgG2a isotype anti-type II collagen, Funakoshi; mouse IgM isotype anti-chondroitin sulfate, Sigma) for 90 min at 37 °C to primarily label the collagens and the proteoglycan at once. The slices were then washed three times in PBS(−) for 10 min and incubated in PBS(−) containing the three secondary antibodies corresponding to each of the primary antibodies (Alexafluor 350-conjugated anti-mouse IgG1 antibody, A21120; Alexafluor 488-conjugated anti-mouse IgG2a antibody, A11001; Alexafluor 568-conjugated anti-mouse IgM antibody, A21043, Invitrogen) for 60 min at 37 °C. Labeled ECM molecules were fluorescently visualized within the cultured cell-agarose construct. The fluorescently stained specimens were mounted on the coverslip and observed using a confocal laser scanning microscope (CLSM; Eclipse; Nikon Corp., Tokyo, Japan).

2.4. Cell viability

The cell viability of individual constructs was assessed at different concentration of the VCs using a previously reported protocol [11]. The cultured constructs were cut into slices with a thickness of approximately 1 mm and washed in PBS(−) for 5 min at 37 °C. These slices were incubated in PBS(−) containing two fluorescent dyes (live cells: Calcein AM, Molecular Probes; dead cells: Ethidium homodimer-1, Molecular Probes) for 15 min at 37 °C. The fluorescently stained constructs were then washed by PBS(−) several times and mounted on the coverslip and observed by CLSM.

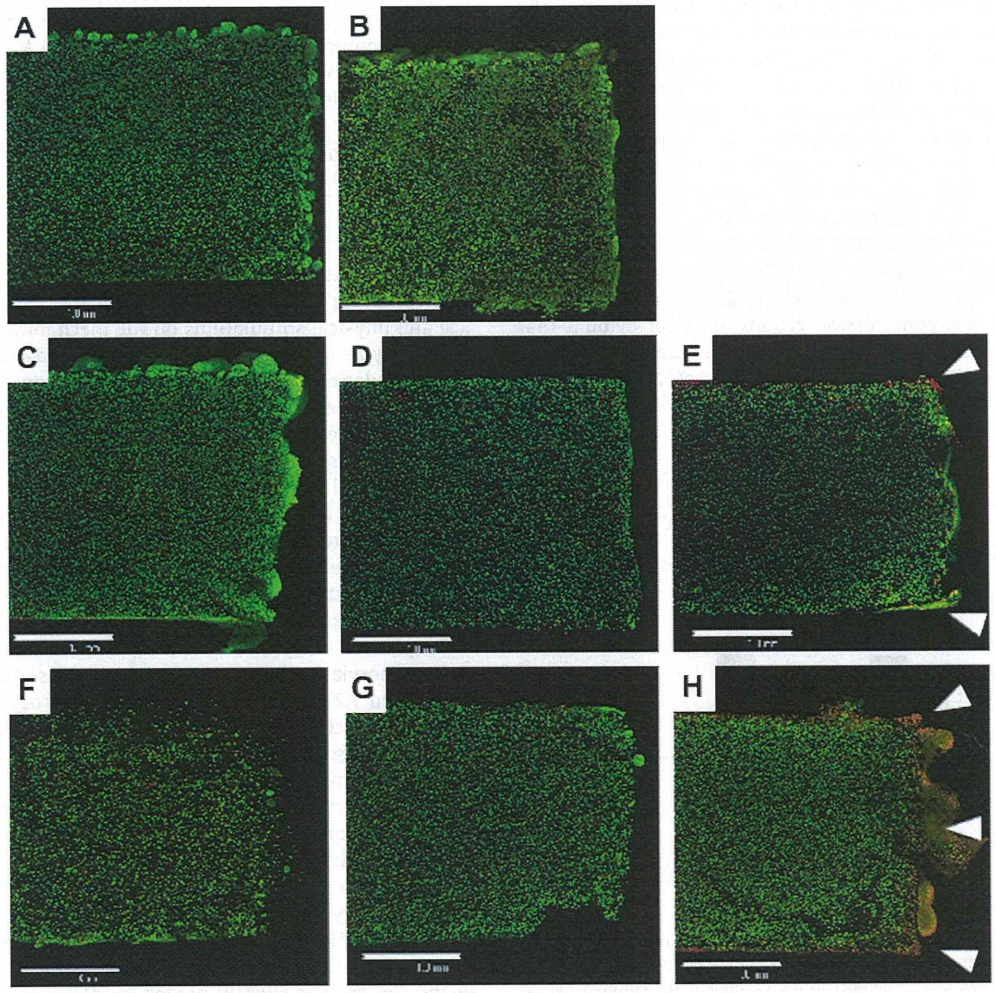

Fig. 2. Low-magnification immunofluorescence images of cell viability under free swelling (A, B, C, F), control (D, G) or compression (E, H) culture conditions. (A): without VC; (B): AsA(2.2); (C–E): A2P(6.4); (F–G): A2P(32). Green represents live cells and red represents dead cells. The culture period was 22 days. Each trichrome-stained sample represents an individual culture. The scale bar represents 1 mm.

2.5. Statistical analysis

Result of the tangent modulus were expressed as the mean ± sample standard deviation (*SD*). The significance of the difference between each experimental group was assayed using the two-tailed Welch's *t*-test. The degree of freedom was abbreviated to *df*. If the results of pairwise comparisons between two groups were *P*-value < 0.01, $d > 1$ and $(1 - \beta) > 0.8$ simultaneously, we judged the difference as significant in the tangent modulus, where *P*-value: level of significance; *d*: Cohen's *d*, an indicator of the effect size [12]; $(1 - \beta)$: the power of the test calculated by R language.

3. Results

3.1. Viability test

In the majority of cases there was a high degree of viability after 22 days of culture, as indicated in Fig. 2. However, some cytotoxicity was evident in the corner of the constructs in two experimental groups, namely A2P(6.4), and most particularly A2P(32), as indicated by the arrow-heads in Fig. 2(E) and (H).

3.2. Measurement of mechanical properties

To evaluate the influence of the mechanical stimulation on the cultured constructs, the tangent moduli of each group after 22 days of culture is shown in Fig. 3. Comparison within the four free-swelling groups only indicated significant differences between the without VC and the AsA(2.2) groups, the latter revealing an increased tangent modulus. By applying cyclic compression to the construct with addition of VC to the culture medium, there was not a clear difference between free-swelling and compression groups for AsA. By contrast, both tangent moduli of the two compression groups were higher than those of several free-swelling samples in each A2P dose group (A2P(6.4) and A2P(32)). Each tangent modulus of the control groups with A2P was ranked against the free-swelling and compression groups. It is not evident that there were differences between each pair of the three compression groups (AsA(2.2), A2P(6.4) and A2P(32)) (AsA(2.2), A2P(6.4): $df = 16$, $P = 0.47$, $d = 0.32$, $(1 - \beta) = 0.030$), but A2P(32) was lower than both AsA(2.2) and A2P(6.4) because each effect size (d) was large but each power ($(1 - \beta)$) was not (AsA(2.2), A2P(32): $df = 25$, $P = 0.017$, $d = 0.99$, $(1 - \beta) = 0.43$; A2P(6.4), A2P(32): $df = 15$, $P = 0.011$, $d = 1.3$, $(1 - \beta) = 0.54$).

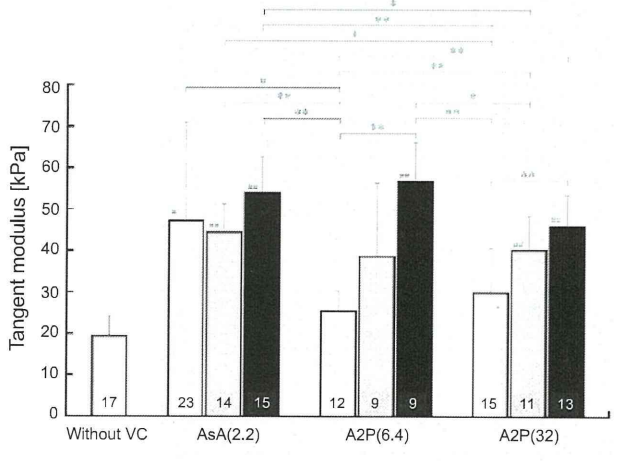

Fig. 3. Comparison of the tangent moduli after 22-day culture period. Cultures were terminated following free-swelling (white column), control (gray), or compression (black) conditions. Each number in the columns is the cultured sample number and each sample represents an individual culture. The error bar represents SD. Sharps (# and ##) and asterisks (* and **) show respective statistical significance between control group and each groups in Welch's *t*-test. #, *: $d > 1$, $P < 0.01$, $(1 - \beta) > 0.8$; ##, **: $d > 2$, $P < 0.01$, $(1 - \beta) > 0.8$.

3.3. Histological observation

Fig. 4 shows immunofluorescent images at low and high magnification revealing the ECM distribution (type I and II collagen and chondroitin sulfate) after 22 days. The high-magnification images were taken in the vicinity of the center of the construct. As indicated in Fig. 4(a) and (A), it is clear that with the absence of VC in the culture medium, there was only a limited amount of ECM. By contrast, in the free-swelling group (AsA(2.2)), there was a fairly uniform distribution of ECM across the construct (Fig. 4(b)). As indicated by the arrows in Fig. 4(B), at high magnification, this revealed a collagen network interconnected between chondrocytes. The low-magnification images for each of the A2P dose groups revealed a similar distribution in ECM across the constructs (Fig. 4(c)–(h)), although it was difficult to observe the ECM in the peripheral region of the compressed construct associated with group A2P(32), as indicated by the arrow-heads in Fig. 4(h). In the high magnification images, type II collagen seems to be interconnected between the chondrocytes, as indicated by the arrow in Figs. 4(E), (G) and (H). However, those examinations revealed that the compression groups of A2P(6.4) and A2P(32) were associated with a more abundant collagen network than the corresponding free-swelling groups. In addition, it is clearly evident that the distribution of chondroitin sulfate is restricted to the peripheral regions of the chondrocytes.

4. Discussion

In order to establish a suitable method for regenerating tissue-engineered cartilage, we studied the effects of two types of chemical and physical stimulations on the mechanical properties of the chondrocyte–agarose construct a regenerated-cartilage model. The first stimulation was the addition of high concentration of VC to the culture medium in order to enhance collagen synthesis. The second was the application of a compressive strain to the construct using a purpose-built bioreactor. Our results show that compressive strain had led to an increase in the tangent modulus and that the collagen network had become dense and interconnected among chondrocytes. We have already described the importance of chondrocyte linkage by ECM for the development of bulk elasticity of the construct in a previous study.

It is well known that even though A2P has no physiological activity, it can nevertheless reproduce the effect of VC activity after dephosphorylation by an alkaline phosphatase (ALP) [13]. Dephosphorylated A2P, or AsA, penetrates chondrocytes through a VC transporter, chiefly the sodium-dependent VC transporter 2 (SVCT2), and supports collagen synthesis as a cofactor in the rough endoplasmic reticulum [14]. In free-swelling culture conditions, we only observed a small number of collagen molecules distributed in the construct. We also observed that the tangent moduli of both A2P dose groups were lower than the moduli of AsA(2.2). We must also consider the reaction rates of both dephosphorylation of A2P by ALP and the transport of AsA into the cytosol via SVCT2. The Michaelis constants of bovine chondrocytes ALP and SVCT2 are 1–10 and 62 ± 25 μM, respectively [15,16]. The affinity of the substrate is slightly higher for ALP than for SVCT2, and as a result, AsA concentration around chondrocytes was lower in the A2P group. The rate of collagen synthesis was also relatively lower in the A2P group than the AsA dose group. Hence, the

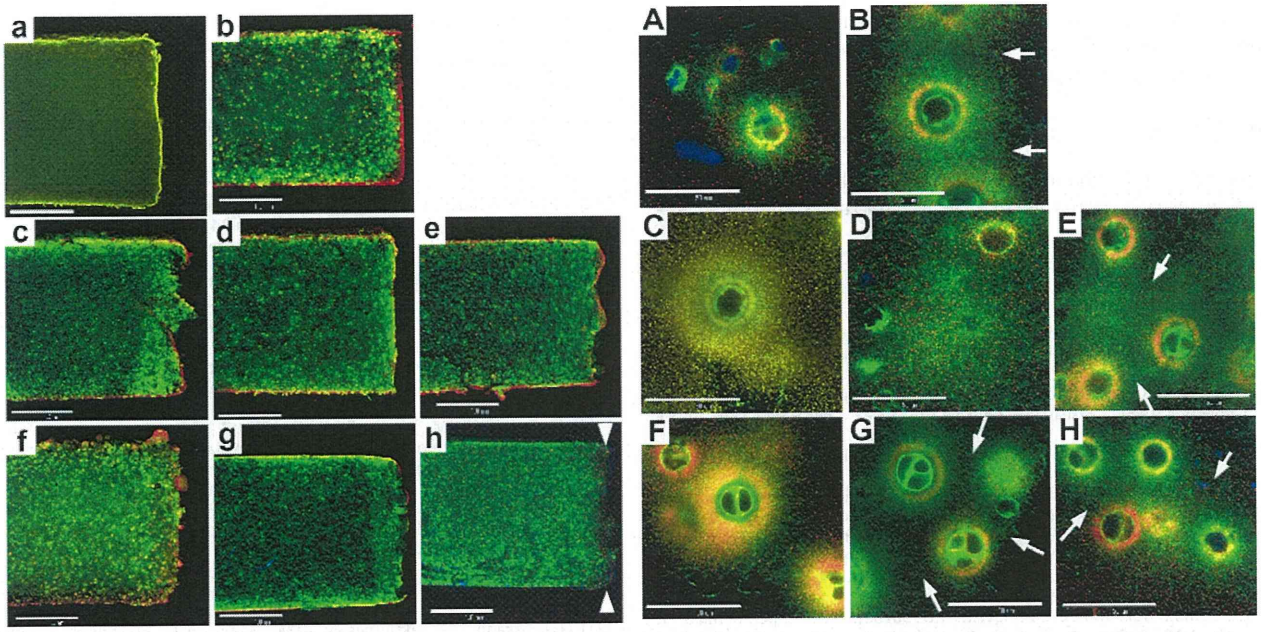

Fig. 4. Low- and high-magnification immunofluorescence images of ECMs under either free-swelling (a, b, c, f, A, B, C, F), control (d, g, D, G), or compression (e, h, E, H) culture conditions. (a, A): without VC; (b, B): AsA(2.2); (c–e, C–E): A2P(6.4); (f–g, F–G): A2P(32). Blue: type I collagen; green: type II collagen; red: chondroitin sulfate. The culture period was 22 days. Scale bars represent 1 mm (a–g) and 50 μm (A–G), respectively. Arrow-heads indicate that we could not observe ECMs at periphery of the tissue of compression group A2P(32). Arrows indicate interconnections among chondrocytes by type II collagen network.

tangent modulus of the free-swelling groups with A2P was suppressed by restraining cytotoxicity of AsA.

When applying compressive strain to the construct, each tangent modulus of A2P(6.4) and A2P(32) was higher than the moduli for the respective free-swelling groups. This is because the collagen network of these groups expanded, which allowed collagen fibers to interconnect among the chondrocytes. We think this mechanical stimulation enhanced diffusion of A2P and nutrients, homogenizing A2P within the construct. In addition, the stimulation probably excited a mechanosensor, activating cell-signaling pathways, namely the mechanotransduction pathways. It is well-known that mechanical stimulation causes chondrocytes to undergo several biological responses involving cartilage remodeling strategies that are relevant to the implantation of cultured tissue [17], e.g., activation of a mitogen-activated protein kinase (MAPK) pathway, a cell-signaling pathway [18,19], an increase in GAG biosynthesis [20], and regulation of inflammatory species synthesis [21]. These chondrocyte responses followed soon after mechanical stimulation and activity of the MAPK pathway was maintained for 5–60 min [18,19]. In synthesizing ECM with mechanical stimulation, chondrocytes built up the collagen network and adapted to changes in the deformation around the cells. Therefore, the compression group with A2P had a higher tangent modulus than the free-swelling group.

The tangent modulus of the compression group with A2P(32) tended to decrease more than the compression group of A2P(6.4) because ECM had been less developed in the peripheral region of A2P(32) than A2P(6.4). Moreover, viability observations revealed that cytotoxicity occurred at the peripheral regions of A2P(32). Generally, we can think that uniaxial compressive deformation of a cylinder model follows the same physics as two-dimensional tension in a plane perpendicular to the axial direction. When the tangent modulus is uniform in the construct, the force at the outer diameter position will be the largest because a reactive force is directly proportionate to the radius. Therefore, less ECM at the peripheral region induced a decrease in the tangent modulus of the construct.

As mentioned above, it is not easy to homogenously develop ECM in free-swelling culture conditions for the purpose of making large-sized regenerated-cartilage tissue. Based on the results of this study, it is necessary to apply mechanical strain to the construct because nutrients should be uniformly supplied. If we also consider the diffusion of nutrients under free-swelling culture conditions, we must note that the diffusion coefficient of water in agarose gel is about 10×10^{-10} m^2s [22,23]. Applying Fick's law, this means that a water molecule diffuses 10 mm per day in the gel. Pluen et al. reported that the diffusion coefficients of proteins in 0.1 M PBS(−) solution, lactalbumin and ovalbumin, were 0.8–1×10^{-10} m^2s [24], and therefore that nutrient particles diffuse 3 mm per day in the gel. Moreover, if the ECM of the cultured construct is dense, it is difficult for nutrients to diffuse in the tissue and the diffusion coefficient will be decreased. Thus, for clinical implantation of a large-sized regenerated-cartilage tissue in order to treat a cartilage defect, the construct should be prepared by applying mechanical stimulation, which would homogenously develop the ECM network.

In summary, this study investigated the influence of two types of VC, AsA and A2P, on the development of the ECM network and regulation of the mechanical properties of chondrocyte–agarose constructs. The collagen network of A2P dose groups improved more than the AsA dose group in free-swelling culture conditions and the tangent modulus of the A2P dose groups did not increase. Moreover, it is clear that free-swelling culture conditions suppressed development of ECM of the inner tissue more than the outer tissue. When applying compressive strain to the construct, tangent moduli of the A2P dose groups were higher due to the fact that ECM networks of the inner tissue had been upregulated with interconnections among the chondrocytes. Additionally, we propose that mechanical stimulation enhanced diffusion of nutrients and improved synthesis of the ECM via mechanotransduction

pathways. We conclude that the application of mechanical stimulation to a large-sized engineered-tissue is necessary for the treatment of articular cartilage defects of various sizes and forms.

Acknowledgments

This study was financially supported by the Grant-in-Aid for Scientific Research from the Japan Society for the Promotion of Science (20360078).

References

[1] R.M. Schulz, A. Bader, Cartilage tissue engineering and bioreactor systems for the cultivation and stimulation of chondrocytes, Eur. Biophys. J. 35 (2007) 539–568.
[2] A. Getgood, R. Brooks, L. Fortier, N. Rushton, Articular cartilage tissue engineering: today's research, tomorrow's practice?, J Bone Joint Surg. Br. 91 (2009) 565–576.
[3] S.R. Frenkel, P.E. Di Cesare, Scaffolds for articular cartilage repair, Ann. Biomed. Eng. 32 (1) (January 2004) 26–34.
[4] J. Farr, B. Cole, A. Dhawan, J. Kercher, S. Sherman, Clinical cartilage restoration: Evolution and overview, Clin. Orthop. Relat. Res. 469 (2011) 2696–2705.
[5] A.H. Gomoll, G. Filardo, L. de Girolamo, J. Esprequeira-Mendes, M. Marcacci, W.G. Rodkey, R.J. Steadman, S. Zaffagnini, E. Kon, Surgical treatment for early osteoarthritis. part I: cartilage repair procedures, Knee Surg. Sports Traumatol. Arthrosc. 20 (2012) 450–466.
[6] A.H. Gomoll, G. Filardo, F.K. Almqvist, W.D. Bugbee, M. Jelic, J.C. Monllau, G. Puddu, W.G. Rodkey, P. Verdonk, R. Verdonk, S. Zaffagnini, M. Marcacci, Surgical treatment for early osteoarthritis. part II: allografts and concurrent procedures, Knee Surg. Sports Traumatol. Arthrosc. 20 (2012) 468–486.
[7] C.M. Revell, K.A. Athanasiou, Success rates and immunologic responses of autogenic, allogenic, and xenogenic treatments to repair articular cartilage defects, Tissue Eng. Part B 15 (2009) 1–15.
[8] S. Omata, Y. Sawae, T. Murakami, Influence of ascorbic acid (asa) concentration in culture medium on mechanical property of regenerated cartilage, J. Environ. Eng. 6 (2011) 416–425.
[9] S. Grad, D. Eglin, M. Alini, M.J. Stoddart, Physical stimulation of chondrogenic cells in vitro: A review, Clin. Orthop. Relat. Res. 469 (2011) 2764–2772.
[10] D.A. Lee, D.L. Bader, Compressive strains at physiological frequencies influence the metabolism of chondrocytes seeded in agarose, J. Orthop. Res. 15 (1997) 181–188.
[11] M.M. Knight, S.R. Roberts, D.A. Lee, D.L. Bader, Live cell imaging using confocal microscopy induces intracellular calcium transients and cell death, Am. J. Physiol. Cell Physiol. 284 (2003) 1083–1089.
[12] J. Cohen, Statistical power analysis for the behavioral sciences, 2nd ed., Lawrence Erlbaum Assoc Inc., New Jersey, 1988.
[13] S. Takamizawa, Y. Maehata, K. Imai, H. Senoo, S. Sato, R. Hata, Effects of ascorbic acid and ascorbic acid 2-phosphate, a long-acting vitamin C derivative, on the proliferation and differentiation of human osteoblast-like cells, Cell Biol. Int. 27 (2004) 255–262.
[14] I. Savini, A. Rossi, C. Pierro, L. Avigliano, M.V. Catani, SVCT1 and SVCT2: key proteins for vitamin C uptake, Amino Acids 34 (2008) 347–355.
[15] A.L. McNulty, T.P. Vail, V.B. Kraus, Chondrocytenext term transport and concentration of ascorbic acid is mediated by SVCT2, Biochim. Biophys. Acta 1712 (2005) 212–221.
[16] R. Fortuna, H.C. Anderson, R.P. Carty, S.W. Sajdera, Enzymatic characterization of the chondrocytic alkaline phosphatase isolated from bovine fetal epiphyseal cartilage, Biochim. Biophys. Acta 570 (1979) 291–302.
[17] L. Ramage, G. Nuki, D.M. Salter, Signalling cascades in mechanotransduction: cell-matrix interactions and mechanical loading, Scand. J. Med. Sci. Sports 19 (2009) 457–469.
[18] J.B. Fitzgerald, M. Jin, D. Dean, D.J. Wood, M.H. Zheng, A.J. Grodzinsky, Mechanical compression of cartilage explants induces multiple time-dependent gene expression patterns and involves intracellular calcium and cyclic AMP, J. Biol. Chem. 279 (2004) 19502–19511.
[19] J.B. Fitzgerald, M. Jin, D.H. Chai, P. Siparsky, P. Fanning, A.J. Grodzinsky, Shear- and compressioninduced chondrocyte transcription requires MAPK activation in cartilage explants, J. Biol. Chem. 283 (2008) 6735–6743.
[20] J.D. Kisiday, J.H. Lee, P.N. Siparsky, D.D. Frisbie, C.R. Flannery, J.D. Sandy, A.J. Grodzinsky, Catabolic responses of chondrocyte-seeded peptide hydrogel to dynamic compression, Ann. Biomed. Eng. 37 (2009) 1368–1375.
[21] O.O. Akanji, P. Sakthithasan, D.M. Salter, T.T. Chowdhury, Dynamic compression alters NFκB activation and IκB-α expression in IL-1β-stimulated chondrocyte/agarose constructs, Inflamm. Res. 59 (2010) 41–52.
[22] E. Davies, Y. Huang, J.B. Harper, J.M. Hook, D.S. Thomas, I.M. Burgar, P.J. Lillford, Dynamics of water in agar gels studied using low and high resolution 1H NMR spectroscopy, Int. J. Food Sci. Technol. 45 (2010) 2502–2507.
[23] N.O. Gustafsson, B. Westrin, A. Axelsson, G. Zacchi, Measurement of diffusion coefficients in gels using holographic laser interferometry, Biotechnol. Progr. 9 (1993) 436–441.
[24] A. Pluen, P.A. Netti, R.K. Jain, D.A. Berk, Diffusion of macromolecules in agarose gels: comparison of linear and globular configurations, Biophys. J. 77 (1999) 542–552.

Colloids and Surfaces B: Biointerfaces 99 (2012) 1–6

Contents lists available at SciVerse ScienceDirect

Colloids and Surfaces B: Biointerfaces

journal homepage: www.elsevier.com/locate/colsurfb

Cell adhesion control on photoreactive phospholipid polymer surfaces

Batzaya Byambaa[a,c], Tomohiro Konno[a,*], Kazuhiko Ishihara[a,b,c]

[a] Department of Bioengineering, School of Engineering, The University of Tokyo, 7-3-1, Hongo, Bunkyo-ku, Tokyo 113-8656, Japan
[b] Department of Materials Engineering, School of Engineering, The University of Tokyo, 7-3-1, Hongo, Bunkyo-ku, Tokyo 113-8656, Japan
[c] School of Engineering and Center for Medical System Innovation, The University of Tokyo, 7-3-1, Hongo, Bunkyo-ku, Tokyo 113-8656, Japan

ARTICLE INFO

Article history:
Available online 7 September 2011

Keywords:
Stimuli-responsive
Photoreactive polymer
Phospholipid polymer
Photocleavable
Cell attachment
Cell detachment

ABSTRACT

Non-invasive and effective cell recovery from culture substrates is important for the passage and characterization of cells. In this study, a photoreactive polymer surface, which uses UV-irradiation to control substrate cell adhesion, was prepared. The photoreactive phospholipid polymer (PMB-PL) reported herein, was composed of a both 2-methacryloyloxyethyl phosphorylcholine (MPC) unit as a cytocompatible unit and methacrylate bearing a photolabile nitrobenzyl group. The PMB-PL polymer was used to coat a cell culture substrate thus affording a photoreactive surface. Surface analysis of the PMB-PL coating indicated a strong photoresponse owing to the sensitivity of the PL unit. Before light exposure, the PMB-PL surface provided cell adhesion. Following UV-irradiation, the PMB-PL coating was converted to a neutral ζ-potential and hydrophilic surface. The photoreactive surface conversion process allowed for the detachment of adhered cells from the PMB-PL surface while maintaining cell viability. This study demonstrates the promise and significance of the PMB-PL photoreactive surface as a method to control cell attachment and detachment for cell function investigation.

1. Introduction

Recently many researchers have shown interest in stimuli-responsive surfaces for cell engineering and other applications. The properties of such "smart surfaces" are effortlessly tuned using an external stimulus [1–5]. Control of cell attachment and detachment from a substrate with continued bioactivity is important for *in vitro* cell culture analysis. The stimuli-responsive surface properties that are of interest for cell engineering development include wettability, hydrophobicity, and hydrophilicity. Previously reported surfaces were responsive to electrical [6–9], temperature [10–12], pH [13–15], or light [16–18] external stimuli. Among the stimuli, light is regarded as ideal for increased spatial and temporal resolution control.

To achieve controlled cell attachment/detachment behavior under mild conditions, it is important to suppress non-specific biomolecule interactions. We have previously reported the 2-methacryloyloxyetyl phosphorylcholine (MPC) polymers that have excellent cytocompatibility due to the inhibition of non-specific biomolecule interactions [19]. These polymers have been widely applied in various fields within the life sciences, including the area of cell engineering materials [20–23]. The MPC polymers effectively suppress the typical inflammatory reaction of adhered cells [23]. Previously, a photo-functionalized MPC polymer bearing photoreactive moieties such as azidophenyl groups and photocleavable linkers were reported to prepare micropattern surfaces for cell adhesion control [24–27].

In this study, we prepared another photoreactive MPC polymer, which controls cell detachment using UV-irradiation. The 2-nitrobenzyl moiety is a typical photocleavable protective group for surface modification, which is cleaved by UV-irradiation ($\lambda = 365$ nm) using a mercury lamp [28]. Incorporating a photoreactive MPC polymer bearing a photocleavable (PL) monomer afforded the PMB-PL polymer. Upon UV-irradiation the cell adhesive molecules were converted at the PMB-PL surface and cell detachment was achieved. In this report, characterization of the PMB-PL polymer and cell attachment/detachment behavior at the surface were investigated.

2. Materials and methods

The MPC was purchased from NOF (Tokyo, Japan), which synthesized the product using the previously reported method [29]. Methacryloyl chloride was purchased from Wako Pure Chemical Industries, Ltd. (Osaka, Japan). The photolabile linker, 4-[4-(1-Hydroxyethyl)-2-methoxy-5-nitrophenoxy]butyric acid was purchased from Sigma–Aldrich Corp. (St. Louis, MO, USA). Other organic reagents were purchased with the highest available purity and were used without further purification.

* Corresponding author at: Department of Bioengineering, The University of Tokyo, 7-3-1, Hongo, Bunkyo-ku, Tokyo 113-8656, Japan.
E-mail address: konno@bioeng.t.u-tokyo.ac.jp (T. Konno).

0927-7765/$ – see front matter © 2011 Elsevier B.V. All rights reserved.
doi:10.1016/j.colsurfb.2011.08.029

HeLa (*Homo sapiens* epithelial cell line established from a uterine cervix carcinoma) and L929 cells (murine fibroblast cell line established from connective tissue) were purchased from Riken Cell Bank (Ibaraki, Japan). The cells were cultured in Dulbecco's Modified Eagle Medium, (DMEM Sigma, St. Louis, MO, USA) with 10% fetal bovine serum, (FBS, Invitrogen Life Technologies, Carlsbad, CA, USA).

2.1. Synthesis of the photocleavable monomer (PL)

The photocleavable monomer (PL) was synthesized under dark conditions using lightproof vials. The photolabile linker, 4-[4-(1-hydroxyethyl)-2-methoxy-5-nitrophenoxy]butyric acid (1.0 mmol) was dissolved in dry dichloromethane (DCM), which had been purged with Ar gas. Both triethylamine (TEA, 3.0 mmol) and methacryloyl chloride (MC, 2.5 mmol), were dissolved in dry DCM and added dropwise to the photolabile linker solution at 0 °C. The solution was stirred overnight at room temperature (RT). The stirred solution was washed with sodium bicarbonate (5%, w/v *aq*), dilute hydrochloric acid (1%, v/v *aq*), and water. The washed solution was evaporated and the remaining liquid product was dissolved in aqueous acetone (50%, v/v *aq*). The reaction mixture was stirred overnight at RT and the liquid monomer was extracted using DCM. The DCM layer was collected, washed with dilute hydrochloric acid (1% v/v, *aq*) and water, dried over magnesium sulfate, and evaporated to yield the photocleavable methacrylate monomer referred to as PL monomer. The structure of the PL monomer was confirmed using ^{1}H NMR (300 MHz, JEOL, Japan). The ^{1}H NMR chart and FT-IR spectrum of PL monomer was shown in Figs. S1 and S2, respectively.

^{1}H NMR (300 MHz, DMSO-*d*6): δ 12.3 (br, $CH_2COO\mathbf{H}$), 7.55 (s, Aromatic-**H**), 7.10 (s, Aromatic-**H**), 6.39, 6.05 (d, d, $OC(dO)CCH_3dC\mathbf{H_2}$), 5.3 (q, Aromatic-C**H**$(CH_3)OC(dO)CCH_3dCH_2$), 4.1 (t, Aromatic-O$\mathbf{CH_2}CH_2CH_2COOH$), 3.95 (s, Aromatic-O$\mathbf{CH_3}$), 2.5 (t, Aromatic-$OCH_2CH_2C\mathbf{H_2}COOH$), 2.1 (s, $OC(dO)CHdCH_2C\mathbf{H_3}$), 1.9 (m, Aromatic-$OCH_2C\mathbf{H_2}CH_2COOH$), 1.55 (d, Aromatic-CHC$\mathbf{H_3}$).

2.2. Synthesis of photocleavable phospholipid polymer (PMB-PL)

The photocleavable phospholipid polymer (PMB-PL) was synthesized via the conventional radical polymerization method using an α,α'-azobisisobutyronitrile (AIBN) initiator. The procedure was completed in a glass tube. The MPC (0.25 mol), BMA (0.50 mol), and photocleavable monomer (0.25 mol) were dissolved in a dioxane/ethanol mixture (1:1 by vol.) at a final concentration of 0.38 M. Thereafter, AIBN (0.38 mM) was added to the solution. The solution was purged with argon gas for 10 min and the glass tube was then sealed. The sealed tube was placed in an oil bath at 60 °C for 48 h. Following polymerization, the PMB-PL was precipitated from diethyl ether/chloroform (3:2 by vol.), and the solid product was collected. The PMB-PL solid was dried overnight, under reduced pressure.

The chemical structure of PMB-PL was confirmed using ^{1}H NMR (300 MHz, JEOL, Tokyo, Japan) and FT-IR (FT-IR 615, JASCO, Tokyo, Japan) spectroscopies. The molecular weight of PMB-PL was measured using a gel-permeation chromatography (GPC) system fitted with an OHpak SB-804HQ column (Shodex®, Showa Denko KK, Tokyo, Japan).

2.3. Surface characterization of PMB-PL

The glass cover slide (18 mm × 18 mm, thickness 0.12–0.17 mm, Matsunami, Tokyo, Japan) was cleaned using ultrasonication in hexane, ethanol, and chloroform solutions at RT for 20 min; then, the slide was treated with oxygen plasma. The glass slides were immersed in a 0.5% (w/v) PMB-PL ethanol solution, and were then dried under reduced pressure. To evaluate the photoreactive property of the PMB-PL surface, a UV-irradiation instrument (Spot-cure SP7, Ushio Inc., Tokyo, Japan) equipped with a 250-W UV lamp (UXM-Q256BY, Ushio Inc., Tokyo, Japan) was used. The power density of the UV source was 80 mW/cm^2.

Surface characterization of the PMB-PL coating was analyzed using Fourier transformed-infrared reflection adsorption spectroscopy (FT-IRRAS), X-ray photoelectron spectroscopy (XPS), static contact angle, ellipsometry, and surface ζ-potential measurement.

A FTIR-500 (JASCO, Tokyo, Japan) was used for the FT-IRRAS spectra measurement. The spectra were obtained under dry conditions at a resolution of 4 cm^{-1} and a scan number of 128.

The XPS spectra were measured using an AXIS-His instrument (Shimadzu/Kratos, Kyoto, Japan) equipped with a monochromatized, Mg-focused, X-ray source. High-resolution scans of C_{1s}, N_{1s}, O_{1s}, P_{2p}, and Si_{2p} were acquired at a photoelectron take-off angle of 90°. The energies in all spectra were corrected using the C_{1s} energy calibration peak at 285 eV.

Static water contact angle measurements were conducted at RT using a CA-W automatic contact-angle meter (Kyowa Interface Science, Tokyo, Japan). The water-in-air and air-in-water systems were applied in this study. In the water-in-air system, the typical protocol involved using a constant drop volume (200 μL) of ultra-pure water onto the surface. For the air-in-water system, the surfaces were horizontally submerged in ultra-pure water. Air bubbles were positioned on the undersides of the surfaces using a syringe equipped with a U-shaped needle. The water drops and air bubbles were monitored using a charge-coupled device (CCD) camera. The captured images were analyzed using FAMAS software (Kyowa Interface Science, Tokyo, Japan) to determine the static contact angle. The contact angle was calculated as the average of more than five values taken at different positions.

The thickness of the PMB-PL was measured under dry conditions using an ellipsometer (alpha-SE®, J.A. Woollam Co., Inc., Lincoln, NE, USA) with a He–Ne laser (632.8 nm) at a 70° incident angle. The refractive indices (n_r) of the Parylene C and poly(MPC) used in the measurement were 1.63 and 1.49, respectively, and both extinction coefficients (k_e) were 0.00. All measurements were conducted under RT air conditions. Data were collected at eight different locations from each sample.

The surface ζ-potential was measured in a 10 mM NaCl solution using a measurement unit (ELS-6000, Photal, Otsuka Electronics Co. Ltd., Osaka, Japan) with an ancillary flat plate cell (10 mm × 30 mm × 60 mm) coated with poly(acrylamide) at 25 °C. Polystyrene latex particles coated with hydroxypropyl cellulose were used as the mobility-monitoring particles.

2.4. Cell attachment/detachment at the PMB-PL surface

HeLa cells were cultured in a 100-mm cell culture dish at 37 °C in 5% CO_2 atmosphere using DMEM containing 10% FBS. After the cells reached sub-confluency, the old media was aspirated; the cells were rinsed with phosphate buffered saline (PBS) and then were exposed to trypsin (1 mL) for 2 min to detach the cells from the surface. The detached cells were added to fresh DMEM, and the cell suspension was centrifuged at 1000 rpm for 3 min. After centrifuging, the supernatant was aspirated and the HeLa cells were suspended in DMEM for the following experiments.

The PMB-PL coated cover-glass surfaces were placed into each well of a 24-well-plate cell-culture dish, sterilized with ethanol, and then washed with PBS. A cell suspension (2.0×10^4 cells/mL, 2 mL) was seeded on the PMB-PL surface and incubated under 5% CO_2 at 37 °C. After incubation for 4 h, unattached cells were washed off with warm fresh medium and the attached cells were observed

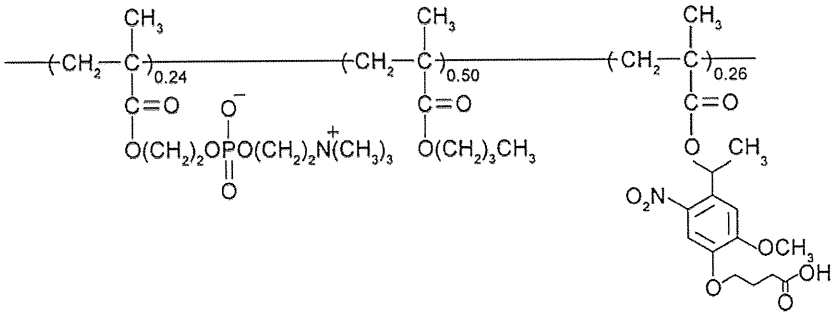

Fig. 1. Chemical structure of photoreactive phospholipid polymer (PMB-PL).

using a phase-contrast microscope. UV light (360 nm, 80 mW/cm^2) was administered to the PMB-PL surface for 60 s. Detached cells following UV-irradiation were recovered and calculated for cell density using a hemocytometer. After irradiation, the culture dish plate was washed with PBS, and the remaining cells were detached using the abovementioned trypsin method. Detached cells were counted and cell counts were converted to cell density per unit area (cells/cm^2).

3. Result and discussion

A photoreactive phospholipid polymer (PMB-PL) was synthesized with MPC, BMA, and PL monomer via the conventional radical polymerization technique. The chemical structure of PMB-PL is shown in Fig. 1. The monomer unit composition of the PMB-PL polymer was calculated by ^{1}H NMR measurement as MPC/BMA/PL = 0.24/0.50/0.26. The PMB-PL was soluble in organic solvents such as alcohol, dimethylsulfoxide, and dioxane. The molecular weight was $M_w = 1.43 \times 10^4$ and average molecular weight was calculated by GPC measurement based on poly(ethylene oxide) (PEO) standards to be M_w/M_n was 1.31.

To evaluate the photochemical activity, PMB-PL was dissolved in ethanol and its spectral change in response to UV light irradiation ($\lambda > 200$ nm) was examined. Before UV irradiation, the solution showed absorption transitions at 300 nm and 348 nm typical for a 3,4-dimethoxy-6-nitrophenyl group [30]. After UV irradiation, the spectrum showed a dose-dependent decrease at the 348-nm transition while two new adsorption transitions appeared at 265 nm and 375 nm. These new adsorption peaks belong to the 4-(4-acetyl-2-methoxy-5-nitrophenoxy)butanoic acid photoproduct, which indicates that the PMB-PL in bulk solution undergoes a photochemical reaction that is characteristic of the 2-nitrobenzyl ester. The PMB-PL after photoirradiation can be soluble in methanol, ethanol, and dimethyl sulfoxide.

The surface of the quartz crystal glass was subjected to UV-ozone treatment, and the glass was immersed in a PMB-PL ethanol solution for several minutes. This process was repeated thrice. After UV irradiation ($\lambda > 200$ nm), the PMB-PL modified glass was washed with distilled water and the UV spectrum was measured. Before UV irradiation, the modified substrate surface showed a similar absorption spectrum between 250 and 400 nm (Fig. 2) as that of the PMB-PL in solution phase. After UV-irradiation, the transition intensity at 348 nm decreased similar to that of PMB-PL

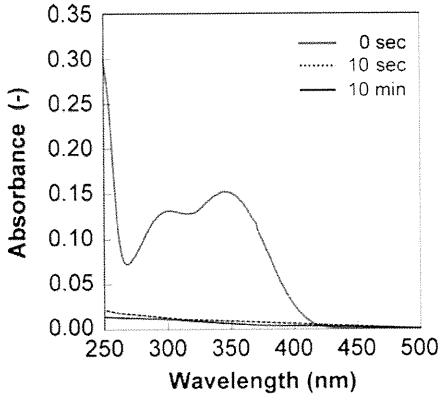

Fig. 2. Absorbance spectra of PMB-PL modified quartz glass surface, which were measured under varied UV-irradiation times.

in bulk solution. However, the transitions at 265 nm and 375 nm corresponding to the elimination of the 4-(4-acetyl-2-methoxy-5-nitrophenoxy)butanoic acid photoproduct by washing, were not observed. These results indicate that the PMB-PL retained its photochemical activity.

The changes in the surface features before and after UV-irradiation are summarized in Table 1. XPS analysis indicated that the PMB-PL modified surface had a phosphorus peak, a nitrogen peak, an oxygen peak, a silicon peak, and a strong carbon peak. After a 10 min UV-irradiation period, the *P/C* ratio on the PMB-PL modified surface increased and the N/C, O/C ratios decreased. These results support the notion that the ester groups on the PMB-PL surface are photocleaved under UV-light.

Ellipsometric measurement revealed that the thickness of the PMB-PL surfaces were 25 ± 7 nm under dry conditions. In addition, from atomic force microscopy (AFM, Nihon Veeco, Tokyo, Japan) observations, the root mean square roughness (RMS) of the PMB-PL surface was calculated as 0.826, which suggests a smooth surface obtained by spin coating (data not shown). The static wettability of the PMB-PL surface was estimated for the air-in-water and water-in-air systems (Table 1). During UV-irradiation of the air-in-water system, the water contact angle ($\beta = 180° - \theta$) was changed from 48° to 34°, which suggests a more hydrophilic surface was observed after 10 min of photolysis. This result indicates that the

Table 1
Changes in PMB-PL surface features before and after UV-irradiation.

PMB-PL surface	Ellipsometric thickness (nm)	Contact angle (°)		*P/C* (-)	ζ-potential (mV)
		Water-in-air	Air-in-water		
Before irradiation	25 ± 7	88	48	0.088	−44.3
After irradiation	25 ± 7	111	34	0.145	−2.1

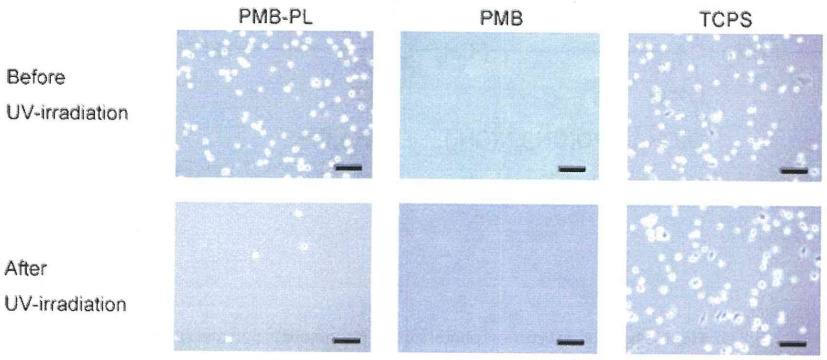

Fig. 3. Phase contrast microscope images (scale = 100 μm) displaying HeLa cells on PMB-PL, PMB, and TCPS surfaces. The upper images were taken before UV irradiation and the lower images were taken following irradiation.

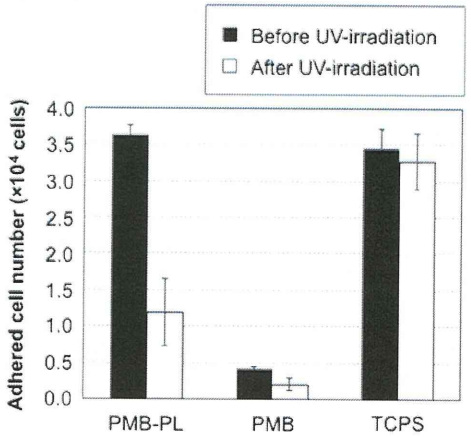

Fig. 4. Adhered cell number on PMB-PL, PMB, and TCPS surfaces shown on left side and detached cell number after UV-irradiation for respective surfaces on right.

surface was mostly converted to the hydrophilic phosphorylcholine (PC) groups, which results from removing the photocleavable PL groups from the substrate. In contrast, for the water-in-air system, the surface static contact angle changed from 88° to 101° which indicates a more hydrophobic surface was obtained after 10 min of light exposure. These results occur because under dry conditions, the PC groups migrate into the inner area and, consequently, leave the hydrophobic butyl methacrylate (BMA) units covered at the uppermost substrate surface. This indicates that surface chemical composition and surface wettability can be controlled using an external UV-light stimulus.

The surface ζ-potential of the PMB-PL surface was −44.3 mV, which is strongly negative. During UV irradiation, the surface ζ-potential changed to −2.1 mV (Table 1), which is a result of an increase in the composition of the MPC unit in the PMB-PL. This increase is attributed to an increase in PL unit photocleavage. It is well reported that the zwitterionic PC groups in PMB-PL surface form an inner salt and thus the electrostatic effects diminish [31–34]. When the composition of the MPC units increased, the surface ζ-potential of the PMB-PL surface was close to zero. This result was in agreement with the results of the static contact angle measurement. From the contact angle measurement and surface ζ-potential measurement, it is concluded that the negatively charged hydrophilic PMB-PL surface is changed to a neutrally charged more hydrophilic surface during UV-photolysis.

Cell attachment and detachment on the PMB-PL surface with UV-irradiation were also examined. In this experiment we used the photoreactive PMB-PL surface, a PMB surface that did not contain the photocleavable PL moiety, and the conventional tissue culture treated polystyrene (TCPS). Fig. 3 shows the phase-contrast

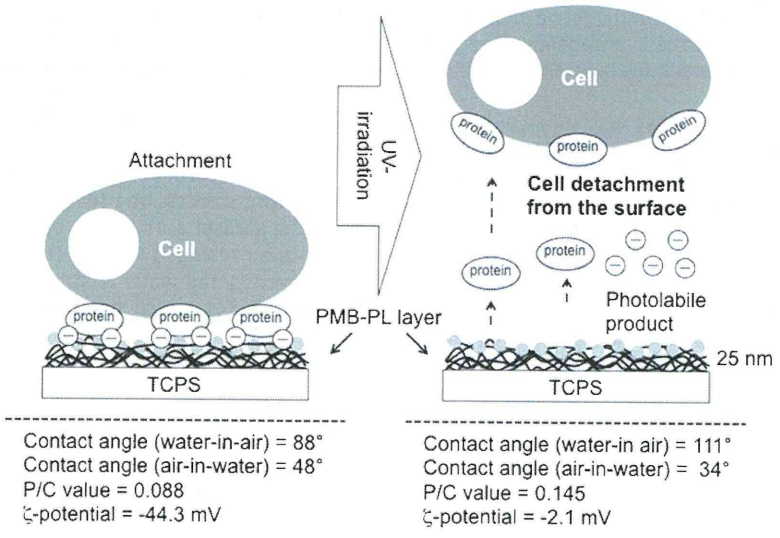

Fig. 5. Schematic of cell attachment/detachment at PMB-PL surface based on alteration of surface properties following UV-irradiation.

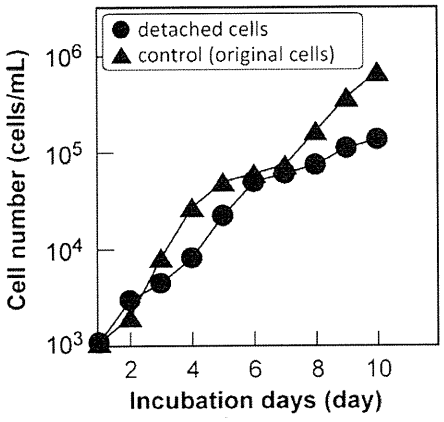

Fig. 6. Cell number dependency on incubation time. The cells were detached from the PMB-PL surface using UV-irradiation.

microscope images of the HeLa cells before and after UV irradiation, and Fig. 4 shows the cell density on each surface before and after irradiation. From the calculations, it was concluded that more than 90% of the seeded cells were attached onto the PMB-PL surface, and 67% of attached cells were detached by photo-irradiation. In the case of the PMB-only surface and the TCPS, less than 5% of the seeded cells were detached following UV-irradiation. This result indicates that UV-exposure induces detachment of attached cells. The proposed mechanism by which this occurs is as follows: the cells are initially bound to the cell-adhesive proteins via the photocleavable PL unit; the PL units are cleaved following the photochemical reaction and the non-biofouling surface of phosphorylcholine groups remain intact at the substrate surface. In generally, the cells were adhered through the adsorbed protein on the substrate. In this study, the cell adhesive experiment was performed in the serum containing medium. Under the condition, it is considered the protein adsorption from the medium is considered to have occurred prior to the cell adhesion. Fig. 5 shows a schematic of cell attachment/detachment processes at the PMB-PL surface based on alteration of the surface properties using UV-irradiation. These results demonstrate the selective detachment of cells at the PMB-PL modified surface, which was related to the photocleavage of the PL unit using UV-irradiation.

Cell attachment and detachment behavior at the PMB-PL surface was also observed using fibroblast cells, L929 (data not shown). These results indicate that the mechanism of cell attachment and detachment on the PMB-PL surface was a consequence of the change in surface properties due to the photocleavage of the PL unit.

We also examined cell proliferation activity after the photoinduced detachment. The detached cells were cultured under usual culture conditions. Fig. 6 shows the cell proliferation of the detached HeLa cells from the PMB-PL surface. The detached cells from PMB-PL after photoirradiation proliferated at the same rate as the normal (original) cells cultured under usual conditions. The PMB-PL detached cells maintained their physiological properties, indicating that the UV-irradiation process did not affect the cell viability, and the PMB-PL surface non-invasively recovered the attached cells.

4. Conclusions

A photoreactive and cytocompatible phospholipid polymer, PMB-PL, was prepared and its surface properties were characterized. The substrate was modified to an extent that it allowed for the study of the photocleaving properties at the surface. Before UV-irradiation, the PMB-PL surface was negatively charged and relatively hydrophobic, which provided protein adsorption and cell adhesion. After irradiation, the surface was neutrally charged and hydrophilic because of the MPC unit. The PMB-PL surface induced cell attachment, and was externally stimulated using UV-light allowing cell detachment from the surface, while maintaining cell viability. Furthermore, the PL monomer unit has a carboxylic group in the side chain, which provides a site for conjugation by desired biomolecules at the PMB-PL surface. The PMB-PL surface is a valuable tool to investigate the bioactivity of conjugated biomolecules, and affords a selective mechanism by which specific cells can be recovered from the surface using UV-light. Selective cell collection and analysis of the cell function at the surface will be reported elsewhere. The development of the PMB-PL surface and the selective detachment of the cells using UV-irradiation has been shown to be a promising and valuable technique for applications in cell analysis and more specifically single-cell analysis.

Acknowledgments

The authors would like to express gratitude to Dr. Hisashi Sugiyama at Hitachi High-Technologies and Mr. Satoshi Ozawa at Central Research Laboratory, Hitachi Co., Ltd. for their valuable discussions.

Appendix A. Supplementary data

Supplementary data associated with this article can be found, in the online version, at doi:10.1016/j.colsurfb.2011.08.029.

References

[1] A.S. Hoffman, Macromol. Symp. 98 (1995) 645.
[2] A.S. Hoffman, Artif. Org. 19 (1995) 458.
[3] P.M. Mendes, Chem. Soc. Rev. 37 (2008) 2512.
[4] N. Nath, A. Chilkoti, Adv. Mater. 14 (2002) 1243.
[5] M.A.C. Stuart, W.T.S. Huck, J. Genzer, M. Müller, C. Ober, M. Stamm, G.B. Sukhorukov, I. Szleifer, V.V. Tsukruk, M. Urban, F. Winnik, S. Zauscher, I. Luzinov, S. Minko, Nat. Mater. 9 (2010) 101.
[6] H. Kaji, M. Kanada, D. Oyamatsu, T. Matsue, M. Nishizawa, Langmuir 20 (2004) 16.
[7] X. Jiang, R. Ferrigno, M. Mrksich, G.M. Whitesides, J. Am. Chem. Soc. 125 (2003) 2366.
[8] W.S. Yeo, M.N. Yousaf, M. Mrksich, J. Am. Chem. Soc. 125 (2003) 14994.
[9] M.N. Yousaf, B.T. Houseman, M. Mrksich, Proc. Natl. Acad. Sci. U.S.A. 98 (2001) 5992.
[10] N. Yamada, T. Okano, H. Sakai, F. Karikusa, Y. Sawasaki, Y. Sakurai, Makromol. Chem. Rapid Commun. 11 (1990) 571.
[11] T. Okano, N. Yamada, H. Sakai, Y. Sakurai, J. Biomed. Mater. Res. 27 (1993) 1243.
[12] T. Okano, N. Yamada, M. Okuhara, H. Sakai, Y. Sakurai, Biomaterials 16 (1995) 297.
[13] M.D. Wilson, G.M. Whitesides, J. Am. Chem. Soc. 110 (1988) 8718.
[14] M. Motornov, R. Sheparovych, R. Lupitskyy, E. MacWilliams, O. Hoy, Adv. Funct. Mater. 17 (2007) 2307.
[15] N. Ayres, C.D. Cyrus, W.J. Brittain, Langmuir 23 (2007) 3744.
[16] N. Negishi, T. Iida, K. Ishihara, I. Shinohara, Makromol. Chem. Rapid Commun. 2 (1981) 617.
[17] K. Ishihara, S. Kato, I. Shinohara, J. Appl. Polym. Sci. 27 (1982) 4273.
[18] K. Ishihara, M. Kim, I. Shinohara, T. Okano, K. Kataoka, Y. Sakurai, J. Appl. Polym. Sci. 28 (1983) 1321.
[19] J. Nakanishi, Y. Kikuchi, T. Takarada, H. Nakayama, K. Yamaguchi, M. Maeda, J. Am. Chem. Soc. 126 (2004) 16314.
[20] K. Ishihara, H. Nomura, T. Mihara, K. Kurita, Y. Iwasaki, N. Nakabayashi, J. Biomed. Mater. Res. 39 (1998) 323.
[21] K. Ishihara, E. Ishikawa, Y. Iwasaki, N. Nakabayashi, J. Biomater. Sci. Polym. Ed. 10 (1999) 1047.
[22] T. Konno, K. Akita, K. Kurita, Y. Ito, J. Biosci. Bioeng. 100 (2005) 88.
[23] T. Konno, K. Ishihara, Biomaterials 28 (2007) 1770.
[24] S. Sawada, S. Sakaki, Y. Iwasaki, N. Nakabayashi, K. Ishihara, J. Biomed. Mater. Res. 64A (2003) 411.
[25] K. Jang, K. Sato, K. Mawatari, T. Konno, K. Ishihara, T. Kitamori, Biomaterials 30 (2009) 1413.
[26] T. Konno, H. Hasuda, K. Ishihara, Y. Ito, Biomaterials 26 (2005) 1381.
[27] T. Konno, N. Kawazoe, G. Chen, Y. Ito, J. Biosci. Bioeng. 102 (2006) 304.

[28] K. Jang, Y. Xu, Y. Tanaka, K. Sato, K. Mawatari, T. Konno, K. Ishihara, T. Kitamori, Biomicrofluidics 4 (2010) 032208.
[29] S.P. Adams, R.Y. Tsien, Annu. Rev. Physiol. 55 (1993) 755.
[30] K. Ishihara, T. Ueda, N. Nakabayashi, Polym. J. 22 (1990) 355.
[31] J. Ottl, D. Gabriel, G. Marriott, Bioconjug. Chem. 9 (1998) 143.
[32] T. Ueda, K. Ishihara, N. Nakabayashi, J. Biomed. Mater. Res. 29 (1995) 381.
[33] Y. Inoue, J. Watanabe, K. Ishihara, J. Colloid Interface Sci. 274 (2004) 465.
[34] T. Konno, K. Kurita, Y. Iwasaki, N. Nakabayashi, K. Ishihara, Biomaterials 22 (2001) 1883.

Colloids and Surfaces B: Biointerfaces 97 (2012) 70–76

Contents lists available at SciVerse ScienceDirect

Colloids and Surfaces B: Biointerfaces

journal homepage: www.elsevier.com/locate/colsurfb

Simple surface treatment using amphiphilic phospholipid polymers to obtain wetting and lubricity on polydimethylsiloxane-based substrates

Kyoko Fukazawa[a], Kazuhiko Ishihara[a,b,*]

[a] Department of Materials Engineering, School of Engineering, The University of Tokyo, 7-3-1, Hongo, Bunkyo-ku, Tokyo 113-8656, Japan
[b] Department of Bioengineering, School of Engineering, The University of Tokyo, 7-3-1, Hongo, Bunkyo-ku, Tokyo 113-8656, Japan

ARTICLE INFO

Article history:
Received 13 February 2012
Received in revised form 3 April 2012
Accepted 4 April 2012
Available online 13 April 2012

Keywords:
Polydimethylsiloxane
Surface treatment
Phospholipid polymer
Wettability
Lubrication property

ABSTRACT

Simple surface treatment of polydimethylsiloxane (PDMS) substrates was performed using an aqueous-ethanolic solution of amphiphilic phospholipid polymers to reduce the hydrophobic and high friction characteristics of PDMS. The phospholipid polymers, poly(2-methacryloyloxyethyl phosphorylcholine (MPC)-*co*-2-ethylhexyl methacrylate (EHMA)-*co*-2-(*N*,*N*-dimethylamino)ethyl methacrylate) (PMED) and poly(MPC-*co*-EHMA) (PMEH) were synthesized, and the effects of the electric charge of the polymer chain on the stability of the attachment to the PDMS surface was investigated. The polymers were dissolved in a mixed solvent of ethanol and water, and the PDMS samples were treated by a simple dipping method using the polymer solution. Pure ethanol as the solvent was ineffective for the attachment of the polymers to the PDMS surface. It was considered that the hydrophobic interactions and electrostatic attraction forces between the polymer chains and the PDMS surface were too weak for efficient interaction in this solvent. On the other hand, the surface wettability and lubricity of PDMS could be improved by treatment with an aqueous-ethanolic solution of PMED. The static contact angle was decreased from 90° to 20° by this treatment, and the dynamic friction coefficient against a Co–Cr ball was decreased by nearly 80% compared with that of the untreated PDMS. The hydrophobic interactions and electrostatic attraction forces generated by PMED were both essential for the stable adsorption of the polymer layer on PDMS. Furthermore, the solubilized state of the polymers affected the adsorption of the polymer. We concluded that the surface of PDMS could be stably modified using aqueous-ethanolic solutions of PMED without the need for pretreatments.

1. Introduction

Polydimethylsiloxane (PDMS) is one of the most frequently used materials for medical devices such as catheters, endoscopes, dentures, finger joints, and contact lenses owing to its attractive properties such as high flexibility, processability, good mechanical properties, high gas permeability and optical transparency [1–3]. However, the native hydrophobicity, high friction, and biofouling tendency of PDMS limit its applications in biological environments. A number of attempts have been made to decrease the hydrophobicity and suppress the nonspecific adsorptions of PDMS by means of surface modification [4–10]. Oxygen plasma treatment is one such technique that has been widely used for modification of the surface hydrophobicity. However, the hydrophilicity conferred by this process is temporary and the surface recovers its hydrophobic property within a short time [11–13]. In addition, the oxygen plasma cannot be applied to the inner surfaces of thin tubes such as catheters and endoscopes from the viewpoint of mean free path. Surface modification of PDMS using biocompatible polymers represents an alternative technique for changing the surface properties. The use of 2-methacryloyloxyethyl phosphorylcholine (MPC) polymers has proved to be particularly promising for improving the biocompatibility of the surface of biomedical devices [14–17]. MPC polymers contain extremely hydrophilic phosphorylcholine groups in their side chain, and surfaces covered with MPC polymers exhibit good wettability, low friction, and resistance to protein adsorption [18–21]. In fact, MPC polymers have been applied to several medical devices such as artificial hip joints [22,23], implantable blood pumps, cardiovascular stents, and contact lenses. Surface modification of PDMS with MPC has been undertaken in various studies by means of either chemical reaction or physical adsorption. Goda et al. introduced poly(MPC) (PMPC) chains onto the PDMS surface by photoinduced graft polymerization [24,25]. Iwasaki et al. modified the PDMS surface by using well-defined ABA-type triblock copolymers composed of PMPC segments (A) and a central PDMS segment (B) with anchoring vinyl groups. The hydrosilylated PDMS surface reacted with vinyl groups of the B

* Corresponding author at: Department of Materials Engineering, School of Engineering, The University of Tokyo, 7-3-1, Hongo, Bunkyo-ku, Tokyo 113-8656, Japan. Tel.: +81 3 5841 7124; fax: +81 3 5841 8647.
E-mail address: ishihara@mpc.t.u-tokyo.ac.jp (K. Ishihara).

0927-7765/$ – see front matter © 2012 Elsevier B.V. All rights reserved.
http://dx.doi.org/10.1016/j.colsurfb.2012.04.008

blocks [26]. This method successfully improved the surface wettability and lubrication and decreased the biofouling tendency of PDMS. Although the modification of the PDMS surface with MPC via a chemical reaction is a powerful tool for enhancing the properties of PDMS, the process is complex and it is difficult to modify intricately shaped devices after fabrication. More practical methods have been reported by Sibarani et al., who modified the PDMS surface by a simple treatment method [27], and Seo et al., who modified the PDMS surface by swelling–deswelling methods using ABA-type block copolymers composed of PMPC (A) and PDMS (B) segments [28]. The relative simplicity of these processes renders them more applicable than grafting polymerization and chemical reaction processes. However, the disadvantage of these methods is that low-polarity solvents such as chloroform are used for the surface treatment process because of the low surface energy of PDMS. These solvents induce swelling of PDMS, and consequently, this method is unsuitable for tailor-made devices with dimension-specific designs. On the other hand, the adsorption of poly(ethylene oxide)-*block*-poly(propylene oxide)-*block*-poly(ethylene oxide) and poly(L-lysine)-*graft*-poly(ethylene glycol) (PLL-*g*-PEG) on hydrophobic surfaces in aqueous environments has been reported [29–31]. Lee et al. investigated the adsorption behavior of PLL-*g*-PEG on the PDMS surface by changing the molecular weight of the copolymer and varying the solvent parameters such as pH and salt concentration. They suggested that the large number of hydrophobic groups in the copolymer and the extended conformation of the polymer in aqueous solution are associated with the ease of adsorption of the polymer [31]. For surface modification of biomedical devices, stability of the adsorbed polymer layer under aqueous conditions is essential. In general, proteins can be readily adsorbed from an aqueous medium onto various surfaces. Surface adsorption is normally irreversible owing to conformational changes of the proteins on the surface. Although surface adsorption of protein is a complex process, hydrophobic interaction and electrostatic forces generated at the interface are some of the dominant forces [32]. When proteins approach a surface, the water molecules between surrounding proteins and the surface are removed by an entropic effect. This phenomenon induces a conformational change in the proteins, and the proteins are irreversibly adsorbed on the surface by hydrophobic interaction and electrostatic interaction. We hypothesized that a molecular design similar to the protein structure, with hydrophobic portions and electric charges, should be suitable for the surface treatment of PDMS. PDMS is an elastic material, its surface is hydrophobic, and its surface ζ potential is −44.1 mV [27]. Therefore, we chose 2-ethylhexyl methacrylate (EHMA) and 2-(*N*,*N*-dimethylamino)ethyl methacrylate (DMAEMA) as monomer units of the MPC polymer, with the expectation of hydrophobic interactions and electrostatic attraction forces. The objective of this study was to modify the PDMS surface with the MPC polymer by simple treatment from aqueous solution, thereby negating the swelling effects of low-polarity solvents on PDMS. The influence of the electric charge of the polymer chain and the polymer conformation in aqueous solution on the modification of the PDMS surface is investigated herein by varying the ratio of water and ethanol in the mixture used as the solvent.

2. Experimental

2.1. Materials

MPC was synthesized according to a previously reported method [33]. EHMA, DMAEMA and sodium 1-anilino-8-naphtalene sulfonate (ANS-Na) were purchased from Tokyo Kasei Kogyo (Tokyo, Japan). Liquid PDMS (Silpot 184®) and its curing agent were purchased from Toray-Dow Corning Asia Co. The other reagents and solvents were commercially available in extra-pure grade and used without further purification.

2.2. Synthesis of positively charged amphiphilic polymer

Poly(MPC-*co*-EHMA-*co*-DMAEMA) (PMED) and poly(MPC-*co*-EHMA) (PMEH) were synthesized by a conventional radical polymerization method in ethanol using 2,2′-azobisisobutyronitrile (AIBN) as the radical initiator. The polymerization was carried out at 60 °C. The formed polymer was purified by pouring the reaction mixture into an excess volume of ether/chloroform (8/2, v/v) for precipitation. Furthermore, unreacted MPC was removed by crushing the precipitated polymer and washing with water for 2.0 h. The polymer was collected by filtration and lyophilized. The chemical structure of the polymer was confirmed by ^{1}H NMR in CD_3CD_2OD, the molecular weight of the polymer was evaluated by gel permeation chromatography (GPC, Jasco, Tokyo, Japan) using hexafluoroisopropanol (HFIP) as the eluent, and the retention time was compared with that of the poly(methyl methacrylate) standard. The chemical structure of PMED and PMEH is shown in Fig. 1.

2.3. Fluorescence measurement using ANS-Na

The polarity of the PMED and PMEH solutions prepared in a mixed solvent with various ratios of ethanol and water was evaluated by fluorescence measurements using ANS-Na as a probe. The polymers were first completely dissolved in ethanol, and water was then added in a prescribed ratio. Subsequently, ethanolic ANS solution was added to each sample and the mixture kept in a dark place. The final polymer concentration was 1.0 wt% and the ANS-Na concentration was 1.0×10^{-5} M. The internal polarity of the polymer aggregate was estimated using the maximum wavelength from the fluorescence of ANS-Na (λ_{ex} = 350 nm, measurement range = 420–650 nm).

2.4. Preparation of PDMS

The precursor of PDMS and curing agent were mixed in a 10:1 (v/v) ratio. The mixtures were evenly spread on a dish and were placed under vacuum to remove air bubbles. The curing reaction was performed at 60 °C for 4.0 h.

2.5. Treatment process

PMED and PMEH were dissolved in ethanol and water was added in a given ratio. Ethanolic polymer (PMED and PMEH) solutions containing water at ratios of 0, 20, 50, and 80 v/v% were prepared and are hereafter referred to as PMED-0, 20, 50, and 80 and PMEH-0, 20, 50, and 80, respectively. The final polymer concentration was adjusted to 1.0 wt%. All PDMS substrates were washed with ethanol prior to the treatment process. The plates were dipped 5 times for a few seconds into the PMED solution and then dried in air. This process was repeated twice and the plates were then completely dried under vacuum.

2.6. Surface characterization

The hydrophilicity of the PMED- and PMEH-treated PDMS surfaces was evaluated by measurement of the air and water contact angles using a static contact angle goniometer (CA-W; Kyowa Interface Science Co., Tokyo, Japan). Water contact angles (θ_{water}) were measured under dry conditions and the air contact angles (θ_{air}) were measured in water. The PDMS substrate was cut to fit dimensions of 10 mm × 40 mm × 1.0 mm and 10 mm × 20 mm × 0.70 mm for the respective air and water contact angle measurements.

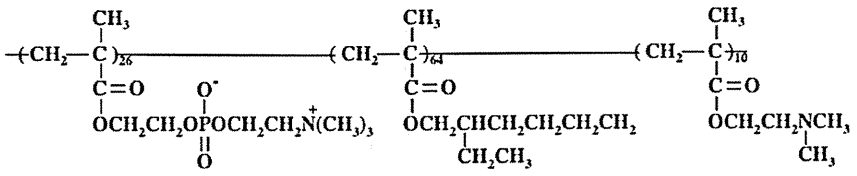

PMED Mw: 2.3×10^5

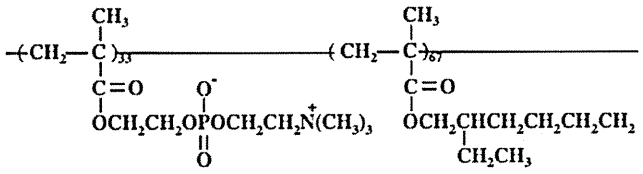

PMEH Mw: 1.2×10^5

Fig. 1. Chemical structure of MPC polymers.

The polymer-treated samples were immersed in water for 1 h and were dried under vacuum before contact angle measurements. In the measurement of θ_{water} under dry conditions, water droplets were brought into contact with the modified PDMS surface and θ_{water} was measured within 10 s using photographic images. θ_{air} was measured in water by attaching the samples to a sample holder, which was then transferred into a glass holder filled with purified water. After 5 min, air bubbles were introduced underneath each sample through U-shaped needles and the contact angles were measured using photographic images. Data were collected at 10 positions for each sample. The stability of the polymer layer was evaluated by immersing the samples in water for 1.0, 24, 72, 120, and 168 h. The surface elemental composition was analyzed using X-ray photoelectron spectroscopy (XPS; AXIS-His165 Kratos/Shimadzu, Kyoto, Japan). The photoelectron take-off angle was fixed at 90°. All of the binding energies were referenced to the C_{1s} peak at 285.0 eV and the corresponding peak areas were used to calculate the respective elemental compositions.

2.7. Friction test

The coefficients of dynamic friction between a Co–Cr ball and the surface of the polymer-treated PDMS samples were measured using a surface property tester (Heidon Type32, Shinto Science Co., Tokyo, Japan). The PDMS substrates were prepared in the box (65 mm × 35 mm × 3.0 mm) and were affixed to the stage. The friction tests were performed in purified water at room temperature with load of 0.98 N, for a maximum of 1.0×10^3 cycles.

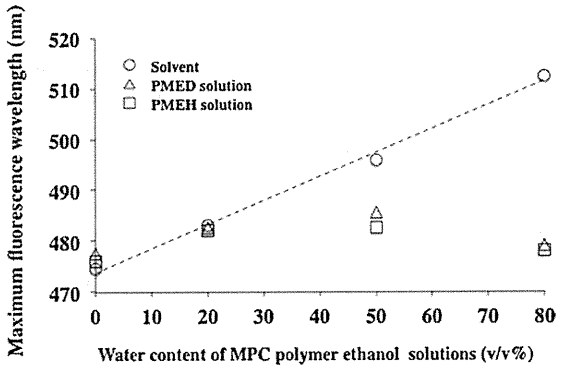

Fig. 2. Peak shifts of ANS-Na fluorescence in MPC polymer solutions.

The scan scale was 20 mm, and the scan speed was 40 mm/s. Three replicate measurements were performed for each sample, and the average values were regarded as the coefficients of dynamic friction.

3. Results and discussion

3.1. Characterization of the solubilized state of PMED in ethanol/water mixture

PMED and PMEH are both soluble in ethanol and do not dissolve in water. In addition, both polymers were soluble in ethanol/water mixtures. The polymer solution was transparent in water con-

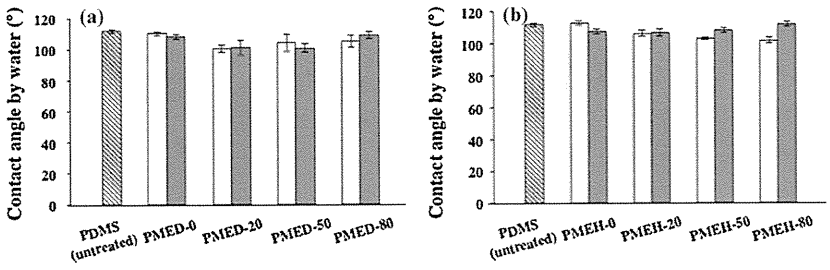

Fig. 3. The contact angles by water on the PDMS surface measured under dry conditions, before and after treatment with PMED (a) and PMEH (b) solution. Open column: just after treatment with the polymer solution. Closed column: after 1.0 h immersion in water.

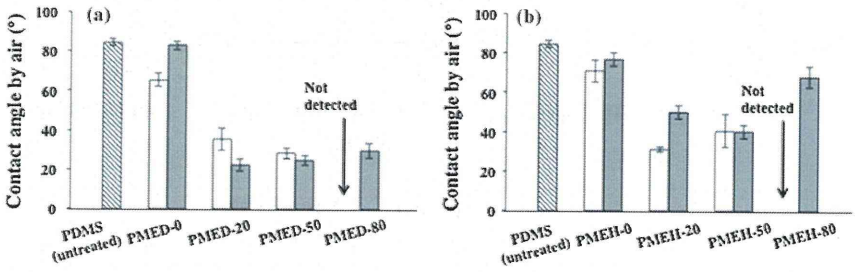

Fig. 4. The contact angles by air on the PDMS surface measured in aqueous solution, before and after coating with PMED (a) and PMEH (b) solution. Open column: just after coating. Closed column: after 1.0 h immersion in water.

tent ranges from 0 v/v% to 80 v/v%. Therefore, the conformation of the polymer changes in ethanol/water mixtures. The solubilized state of PMED and PMEH was evaluated after dissolution in ethanol/water mixtures of various ratios, using ANS-Na as a fluorescence probe. ANS-Na is sensitive to solvent polarity; the fluorescence quantum yield of ANS-Na is enhanced in hydrophobic environments, with a concomitant blue shift of the emission maximum [34]. Fig. 2 shows the emission maximum of ANS-Na in the solvent, PMED solution and PMEH solution. The maximum wavelength of fluorescence (λ_{max}) of ANS-Na in the 80 v/v% aqueous ethanolic solvent was 505 nm. However, the peak was blue-shifted with decreasing content of water. The λ_{max} of ANS-Na was almost the same in both the PMED and PMEH solutions. In the purely ethanolic and 20 v/v% aqueous-ethanolic polymer solutions, the λ_{max} of ANS-Na was almost same as that in the solvent. On the other hand, in the 50 v/v% and 80 v/v% aqueous-ethanolic polymer solutions, the λ_{max} was considerably lower than that in the solvent. The ratio of hydrophilic to hydrophobic units is almost same in both PMED and PMEH. These results indicate that both of the polymers undergo aggregation with increasing water content by hydrophobic interactions. In the 80 v/v% aqueous-ethanolic polymer solution, the polarity of the inside of the polymer aggregate was almost the same as that of ethanol.

3.2. Surface characterization of modified PDMS

The effect of the polymer conformation on the modification of the PDMS surface was investigated after dissolving PMED and PMEH in solvents with different ratios of ethanol to water. Fig. 3 shows the values of contact angles by water (θ_{water}) on the PDMS surface before and after treatment with PMED (a) and PMEH (b). In all samples, high values were obtained for the water contact angles under dry conditions, which were the same as those of untreated PDMS, and the values were not changed after immersion in water for 1 h. The phosphorylcholine group of the MPC polymers is hydrophilic, however, the hydrophobic units of the polymer are enriched at the air interface to decrease the surface free energy [35]. Fig. 4 shows the values of contact angles by air (θ_{air}) on the PDMS surface before and after treatment with PMED (a) and PMEH (b). In contrast to θ_{water} under dry conditions, θ_{air} in water were drastically decreased on the PMED and PMEH-treated surfaces, relative to the untreated surface, with the exception of the surface treated with PMED-0 and PMEH-0 (i.e., purely ethanolic) solutions. θ_{air} could not be measured on the surfaces treated with PMED-80 and PMEH-80, because the air bubble did not attach to the surface. The hydrophilic phosphorylcholine group is exposed in aqueous environments to reduce the interfacial free energy, thus, these results indicate successful treatment of the PDMS surface with PMED-20, 50, and 80 and PMEH-20, 50, and 80. After immersion in water for 1.0 h, the surfaces treated with PMED-20, 50, and 80 maintained their hydrophilicity. However, the contact angles of the surfaces treated with PMEH-20, 50, and 80 were increased after immersion in water for 1.0 h. In particular, the θ_{air} value of the surface treated with PMEH-80 was increased from 0° to 70°. These results indicate that PMEH-20, 50, and 80 were attached to the PDMS surface via weak interactions, and the polymer layer could be easily removed from the PDMS surface during immersion in aqueous solution. The success of the surface treatment with PMED and PMEH was further evaluated by XPS measurement. In the case of the surfaces treated with PMED-20, 50, and 80 and PMEH-20, 50, and 80, ammonium nitrogen and phosphorous peaks were observed at 403 eV and 133 eV, respectively. These atoms were attributed to the MPC unit. On the other hand, there were no peaks in the nitrogen region and phosphorous region for the surfaces treated with PMED-0 and PMEH-0. The results of the XPS and θ_{air} measurements reveal that when ethanol was used as a solvent (in the absence of water), the PDMS surface treatment process was unsuccessful. Fig. 5 shows the relationship between θ_{air} on the PDMS surfaces treated with PMED and PMEH versus the atomic ratio of P/Si of the surface. Contact angle and XPS values after immersion in water for 1.0 h were used for this plot. The atomic ratio of P/Si corresponded to the surface density of the MPC unit; therefore, the density of the phosphorylcholine group could be evaluated on this basis. The contact angle decreased

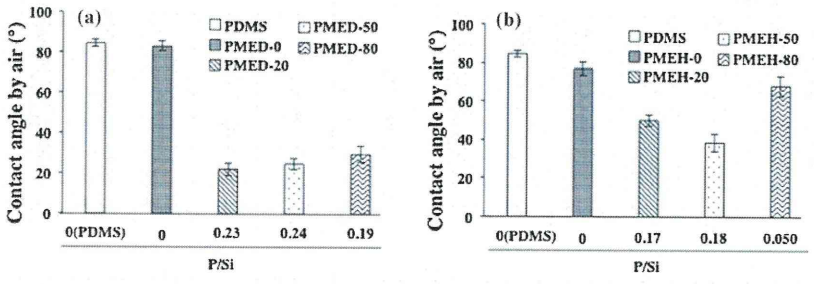

Fig. 5. Atomic ratio of P/Si on the PDMS surface coated with various MPC polymer solutions versus the air contact angles in an aqueous solution.

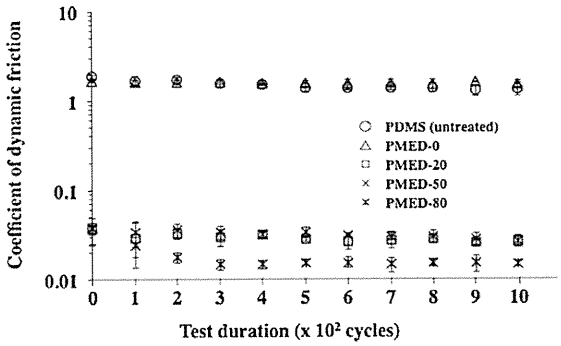

Fig. 6. Time course of the dynamic friction coefficient of the PDMS surface coated with PMED solution.

with an increase in the atomic ratio of P/Si, indicating that the wettability was conferred by the hydrophilic phosphorylcholine group.

3.3. Lubrication property

The lubricity of the surface is important for biomedical devices such as catheters, endoscopes, and artificial joints [19]. The dynamic friction coefficient was used as a parameter for characterizing the lubricity of the PDMS surface treated with PMED in water. Fig. 6 shows the time course of the dynamic friction coefficient between a Co–Cr ball and the surface of PMED-treated PDMS in water. The untreated PDMS surface and PMED-0 treated surface exhibited a very high dynamic friction coefficient of approximately 1.16, consistent with the unsuccessful treatment of the PDMS surface by PMED-0 indicated by the XPS and contact angle measurements. However, after treatment with PMED-20, 50, and 80, the dynamic friction coefficient was dramatically decreased to approximately 0.030, 0.030, and 0.015, respectively. This decrease is attributed to elimination of strong hydrophobic interactions by treatment with hydrophilic PMED. The hydrophilic state ensures the formation of an aqueous lubrication layer and reduces the friction force. The results of the lubrication tests corroborate with the results of the contact angle measurements. Furthermore, the low friction coefficient was maintained during 1.0×10^3 cycles at 0.98 N, demonstrating the stability of the PMED layer formed on the PDMS substrate during the treatment process.

3.4. Stability of MPC polymer on PDMS surface

The stability of the PMED and PMEH layers on the PDMS substrate in aqueous environments was further evaluated by XPS following surface treatment. Fig. 7 shows time course of the elemental ratio of P/Si for the PDMS surfaces treated with PMED (a) and PMEH (b). After immersion in water for 24 h, the atomic ratio of P/Si on the surface treated with PMED-50 and 80 decreased from 0.25 to 0.10. On the other hand, the atomic ratio of P/Si was maintained at 0.25 on the surface treated with PMED-20. All of the treated surfaces maintained an atomic ratio of P/Si of approximately 0.05 over the course of 168 h.

We have previously expounded the relationship between the amount of adsorbed fibrinogen and the surface P/Si ratio [36]. From that study, it is known that the fibrinogen adsorption capacity of the untreated PDMS surface is approximately 1.9 $\mu g/cm^2$. The amount of adsorbed fibrinogen was found to decrease with an increase in the atomic ratio of P/Si. In the case of a surface having an atomic ratio of P/Si of 0.035, the amount of fibrinogen adsorbed was significantly reduced to approximately 75% of that observed for the untreated PDMS. On this basis, it is predicted that the surface treated with PMED should exhibit good biofouling resistance after immersion in water for 168 h.

For the surfaces treated with PMEH-20 and 50, the atomic ratio of P/Si decreased from 0.25 to below 0.05 after immersion in water for 24 h, and for the surface treated with PMEH-80, the decrease was even more drastic, moving from approximately 0.15 to 0.05 over an immersion period of only 1.0 h. The P/Si ratio declined to almost 0 after immersion in water for 72 h for all of the treated surfaces. The pK_a of poly(DMAEMA) is about 8.0 [37,38]. In water (pH 5.6), more than 90% of the dimethyl amino groups are protonated. Therefore, PMED is positively charged and was more strongly adsorbed than PMEH; in particular, PMED-20 exhibited the highest stability among all the tested PMED types.

Fig. 8 shows an illustration of the relationship between the solubilized state of the polymer and the adsorption behavior of the polymer on the PDMS substrate. On the basis of the fluorescence measurements using ANS-Na, it was evident that neither PMED nor PMEH could form hydrophobic domains in the purely ethanolic and 20 v/v% aqueous-ethanolic solutions. On the other hand, hydrophobic domains were formed in the 50 v/v% and 80 v/v% aqueous-ethanolic solutions. In purely ethanolic solution, the hydrophobic interaction and electrostatic attraction forces were not operative between the polymer chains and the PDMS surface, therefore, there was no attachment of PMED and PMEH to the surface. In the 20 v/v% aqueous-ethanolic solutions of both polymers, the polymer chains were in the stretched conformation, and were adsorbed on the PDMS surface via hydrophobic interactions. However, the stability of the PMED layer on the surface was much higher than that of the PMEH layer. PMED possesses positive charges in the aqueous solution based on the DMAEMA units, whereas the PDMS surface is negatively charged. Therefore, the difference in the stability of the layers formed by PMED and PMEH suggests that PMED is adsorbed onto the PDMS surface not only by hydrophobic interactions but also by electrostatic attraction forces. In 50 v/v% and 80 v/v% aqueous-ethanolic solutions, PMED and PMEH could form aggregates, with hydrophobic interaction operating as the driving force for aggregation of the hydrophobic units. Because the hydrophobic domain was formed inside the polymer aggregate

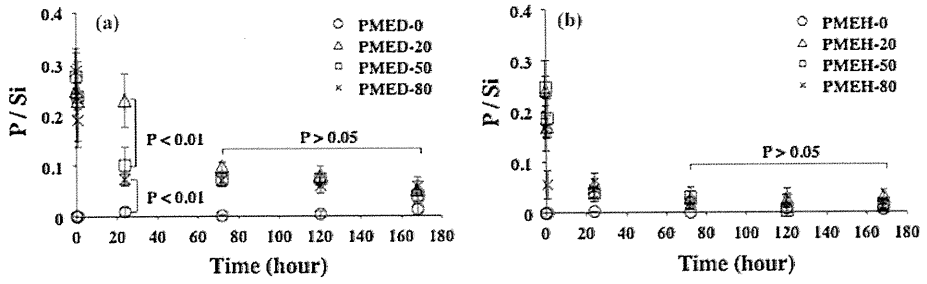

Fig. 7. Time course of the atomic ratio of P/Si on the PDMS surface coated with PMED (a) and PMEH (b) solution.

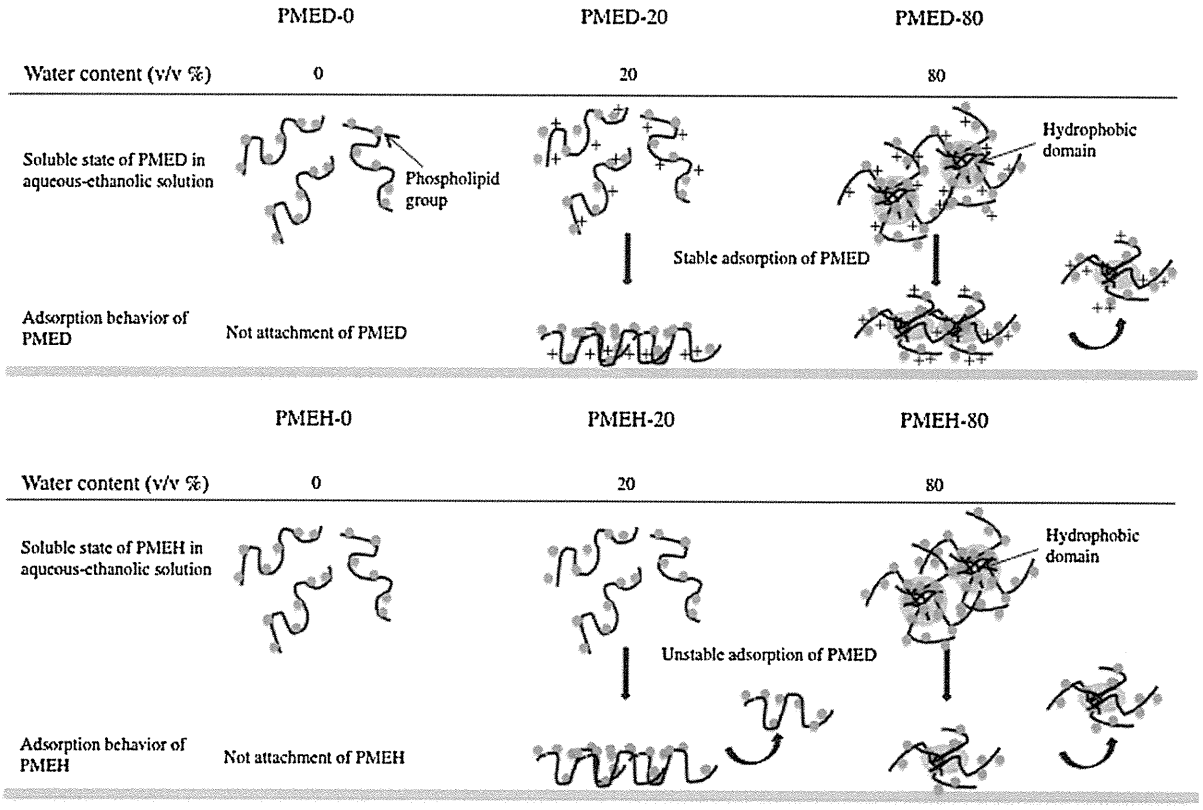

Fig. 8. Schematic illustration of the conformation of PMED and PMEH in aqueous-ethanolic solution and adsorption behavior of PMED and PMEH at PDMS surface.

and the hydrophobic interaction between the polymer chains and the PDMS surface was weakened, PMEH was weakly adsorbed on the PDMS surface. On the other hand, PMED was adsorbed on the PDMS surface primarily via electrostatic forces. Thus, PMED and PMEH may attach to the PDMS surface via either hydrophobic interaction or electrostatic attraction forces. However, both interactions are essential for stable binding between the polymer chains and the PDMS surface. The conformation of a protein is changed after adsorption; the hydrophobic inner surfaces are turned to the outside, and hydrophobic interaction between amino residues and the surface becomes stronger. This is due to the flexible and fragile conformation of proteins. The polymer aggregate is rigid and thermodynamically stable; therefore, the hydrophobic inner region cannot be turned to the outside after adsorption. Thus, the polymer must exist as discrete units in aqueous solution for formation of a stable surface layer, because the hydrophobic interaction between the polymer chains and the surface is weak in the aggregated state.

4. Conclusion

The surface properties of PDMS were readily modified by a simple treatment process using aqueous-ethanolic PMED and PMEH solutions without the need for any pretreatment process. After treatment, the PDMS surface exhibited good water wettability and the dynamic friction coefficient of the surface was decreased by nearly 80% compared with that of the untreated PDMS surface. We demonstrated that the positive charge and hydrophobic moiety were both needed in the polymer for the formation of a stable treatment during treatment of PDMS. Further, we found that the conformation of the polymer in solution influenced the adsorption process. This treatment process is simple and it is possible to apply to various devices made of PDMS after fabrication.

References

[1] M. Chhabra, J.M. Prausnitz, C.J. Radke, Biomaterials 28 (2007) 4331.
[2] M.K. Horne III, K.J. Brokaw, Thromb. Res. 112 (2003) 111.
[3] T.J. Joyce, A. Unsworth, Wear 250 (2001) 199.
[4] J.G. Alauzum, S. Young, R. D'Souza, L. Liu, M.A. Book, H.D. Sheardown, Biomaterials 31 (2010) 3471.
[5] A. Wu, B. Zhao, Z. Dai, J. Qin, B. Lin, Lab Chip 6 (2006) 942.
[6] Y. Yuan, X. Zang, F. Ai, J. Zhou, J. Shen, S. Lin, Polym. Int. 53 (2004) 121.
[7] S. Pintro, P. Alves, C.M. Matos, A.C. Santos, L.R. Rodrigues, J.A. Teixeira, M.H. Gil, Colloids Surf. B: Biointerfaces 81 (2010) 20.
[8] H. Makamba, Y.Y. Hsieh, W.C. Sung, S.H. Chen, Anal. Chem. 77 (2005) 3971.
[9] M. Farrell, S. Beaudoin, Colloids Surf. B: Biointerfaces 81 (2010) 468.
[10] H. Chen, Z. Zhang, Y. Chen, M.A. Brook, H.D. Sheardown, Biomaterials 26 (2005) 2391.
[11] M. Ouyang, C. Yuan, R.J. Muisener, A. Boulares, J.T. Koberstein, Chem. Mater. 12 (2000) 1591.
[12] D. Bodas, C.K. Malek, Microelectr. Eng. 83 (2006) 1277.
[13] M. Morra, E. Occhiello, R. Marola, F. Garbassi, P. Humphrey, D. Johnson, J. Colloid Interface Sci. 137 (1990) 11.
[14] Y. Inoue, T. Nakanishi, K. Ishihara, React. Funct. Polym. 71 (2011) 350.
[15] R. Matsuno, K. Ishihara, NanoToday 6 (2011) 61.
[16] K. Ishihara, N.P. Ziats, B.P. Tierney, N. Nakabayashi, J.M. Anderson, J. Biomed. Mater. Res. 25 (1991) 1397.
[17] K. Ishihara, H. Nomura, T. Mihara, K. Kurita, Y. Iwasaki, N. Nakabayashi, J. Biomed. Mater. Res. 39 (1998) 323.
[18] M. Kyomoto, Y. Iwasaki, T. Moro, T. Konno, F. Miyaji, H. Kawaguchi, Y. Takatori, K. Nakamura, K. Ishihara, Biomaterials 28 (2008) 3121.
[19] M. Kyomoto, T. Moro, K. Saiga, F. Miyaji, H. Kawaguchi, Y. Takatori, K. Nakamura, K. Ishihara, Biomaterials 31 (2010) 658.
[20] S.H. Ye, C.A. Johnson Jr., J.R. Woolley, H. Murata, L.J. Gamble, K. Ishihara, W.R. Wagner, Colloids Surf. B: Biointerfaces 79 (2010) 357.
[21] T. Simizu, T. Goda, N. Minoura, M. Takai, K. Ishihara, Biomaterials 31 (2010) 3274.
[22] T. Moro, Y. Takatori, K. Ishihara, T. Konno, Y. Takigawa, T. Matsushita, U.I. Chung, K. Nakamura, H. Kawaguchi, Nat. Mater. 3 (2004) 829.
[23] T. Moro, H. Kawaguchi, K. Ishihara, M. Kyomoto, T. Karita, H. Ito, K. Nakamura, Y. Takatori, Biomaterials 30 (2009) 2995.

[24] T. Goda, T. Konno, M. Takai, T. Moro, K. Ishihara, Biomaterials 27 (2006) 5151.
[25] T. Goda, R. Matsuno, T. Konno, M. Takai, K. Ishihara, Colloids Surf. B: Biointerfaces 63 (2008) 64.
[26] Y. Iwasaki, M. Takamiya, R. Iwata, S. Yusa, K. Akiyoshi, Colloids Surf. B: Biointerfaces 57 (2007) 226.
[27] J. Sibarani, M. Takai, K. Ishihara, Colloids Surf. B: Biointerfaces 54 (2007) 88.
[28] J.H. Seo, R. Matsuno, T. Konno, M. Takai, K. Ishihara, Biomaterials 29 (2008) 1367.
[29] A. Lee, N.D. Spencer, Tribol. Int. 38 (2005) 922.
[30] S. Lee, R. Iten, M. Muller, N.D. Spencer, Macromolecules 37 (2004) 8349.
[31] S. Lee, N.D. Spencer, Langmuir 24 (2008) 9479.
[32] M. Rabe, D. Verdes, S. Seeger, Adv. Colloid Interface Sci. 162 (2011) 87.
[33] K. Ishihara, T. Ueda, N. Nakabayashi, Polym. J. 22 (1990) 355.
[34] T. Konno, J. Watanabe, K. Ishihara, Biomacromolecules 5 (2004) 342.
[35] K. Futamura, R. Matsuno, T. Konno, M. Takai, K. Ishihara, Langmuir 24 (2008) 10340.
[36] K. Ishihara, B. Ando, M. Takai, Nanobiotechnology 3 (2007) 83.
[37] M.J. Bruining, H.G.T. Blaauwgeers, R. Kuijer, E. Pels, R.M.M.A. Nuijts, L.H. Koole, Biomaterials 21 (2000) 595.
[38] A.M. Funhoff, C.F.V. Nostrum, G.A. Koning, N.M.E.S. Nieuwenbroek, D.J.A. Crommelin, W.E. Hennink, Biomacromolecules 5 (2004) 32.